Atmos. Meas. Tech., 13, 2523–2546, 2020
https://doi.org/10.5194/amt-13-2523-2020
© Author(s) 2020. This work is distributed under
the Creative Commons Attribution 4.0 License.

Atmospheric Measurement Techniques
Open Access

Assessment of NO_2 observations during DISCOVER-AQ and KORUS-AQ field campaigns

Sungyeon Choi[1,2], Lok N. Lamsal[1,3], Melanie Follette-Cook[1,4], Joanna Joiner[1], Nickolay A. Krotkov[1], William H. Swartz[5], Kenneth E. Pickering[1,6], Christopher P. Loughner[7], Wyat Appel[8], Gabriele Pfister[9], Pablo E. Saide[10], Ronald C. Cohen[11], Andrew J. Weinheimer[9], and Jay R. Herman[1,12]

[1]NASA Goddard Space Flight Center, Greenbelt, MD 20771, USA
[2]Science Systems and Applications, Inc., Lanham, MD 20706, USA
[3]Universities Space Research Association, Columbia, MD 21046, USA
[4]Goddard Earth Sciences Technology and Research, Morgan State University, Baltimore, MD 20251, USA
[5]Johns Hopkins University, Applied Physics Laboratory, Laurel, MD 20723, USA
[6]Department of Atmospheric and Oceanic Science, University of Maryland, College Park, MD 20742, USA
[7]NOAA Air Resources Laboratory, College Park, MD 20740, USA
[8]Environmental Protection Agency, Research Triangle Park, NC 27709, USA
[9]National Center for Atmospheric Research, Boulder, CO 80301, USA
[10]Department of Atmospheric and Oceanic Sciences, and Institute of the Environment and Sustainability, University of California, Los Angeles, CA 90095, USA
[11]Department of Chemistry and Department of Earth and Planetary Science, University of California, Berkeley, CA 94720, USA
[12]Joint Center for Earth Systems Technology, University of Maryland Baltimore County, Baltimore, MD 21250, USA

Correspondence: Sungyeon Choi (sungyeon.choi@nasa.gov)

Received: 6 September 2019 – Discussion started: 18 November 2019
Revised: 24 March 2020 – Accepted: 10 April 2020 – Published: 19 May 2020

Abstract. NASA's Deriving Information on Surface Conditions from Column and Vertically Resolved Observations Relevant to Air Quality (DISCOVER-AQ, conducted in 2011–2014) campaign in the United States and the joint NASA and National Institute of Environmental Research (NIER) Korea–United States Air Quality Study (KORUS-AQ, conducted in 2016) in South Korea were two field study programs that provided comprehensive, integrated datasets of airborne and surface observations of atmospheric constituents, including nitrogen dioxide (NO_2), with the goal of improving the interpretation of spaceborne remote sensing data. Various types of NO_2 measurements were made, including in situ concentrations and column amounts of NO_2 using ground- and aircraft-based instruments, while NO_2 column amounts were being derived from the Ozone Monitoring Instrument (OMI) on the Aura satellite. This study takes advantage of these unique datasets by first evaluating in situ data taken from two different instruments on the same aircraft platform, comparing coincidently sampled profile-integrated columns from aircraft spirals with remotely sensed column observations from ground-based Pandora spectrometers, intercomparing column observations from the ground (Pandora), aircraft (in situ vertical spirals), and space (OMI), and evaluating NO_2 simulations from coarse Global Modeling Initiative (GMI) and high-resolution regional models. We then use these data to interpret observed discrepancies due to differences in sampling and deficiencies in the data reduction process. Finally, we assess satellite retrieval sensitivity to observed and modeled a priori NO_2 profiles. Contemporaneous measurements from two aircraft instruments that likely sample similar air masses generally agree very well but are also found to differ in integrated columns by up to 31.9 %. These show even larger differences with Pandora, reaching up to 53.9 %, potentially due to a combination of strong gradients in NO_2 fields that could be missed by aircraft spirals and errors in the Pandora retrievals. OMI NO_2 values are about a

factor of 2 lower in these highly polluted environments due in part to inaccurate retrieval assumptions (e.g., a priori profiles) but mostly to OMI's large footprint ($> 312\,km^2$).

1 Introduction

Nitrogen dioxide (NO_2) plays an important role in the troposphere by altering ozone production and OH radical concentration (Murray et al., 2012, 2014). It is one of the six United States Environmental Protection Agency (EPA) criteria pollutants because of its adverse health effects on humans (WHO, 2013). Major sources of nitrogen oxides (NO_x=$NO + NO_2$) in the troposphere include combustion, soil, and lightning. As a trace gas with a relatively short lifetime, NO_2 is usually confined to a local scale with respect to its source and therefore exhibits strong spatial and temporal variations, leading to difficulties in comparing NO_2 observations by methods with different atmospheric sampling.

Due to its distinct absorption features at ultraviolet–visible (UV–Vis) wavelengths, atmospheric NO_2 is observable from ground- and space-based remote sensing instruments. In particular, space-based measurements of tropospheric column NO_2 have been widely used to study spatial and temporal patterns (e.g., Beirle et al., 2003; Richter et al., 2005; Boersma et al., 2008; Lu and Streets, 2012; Wang et al., 2012; Hilboll et al., 2013; Russell et al., 2010, 2012; Duncan et al., 2013; Lin et al., 2015) as well as long-term trends (e.g., van der A et al., 2008; Lamsal et al., 2015; Krotkov et al., 2016), and to infer NO_x sources (e.g., Jaeglé et al., 2005; van der A et al., 2008; Bucsela et al., 2010; de Wildt et al., 2012; Lin, 2012; Ghude et al., 2010; Ghude et al., 2013a; Mebust and Cohen, 2013; Pickering et al., 2016) and top-down NO_x emissions (e.g., Martin et al., 2003; Konovalov et al., 2006; Zhao and Wang, 2009; Lin et al., 2010; Lamsal et al., 2011; Ghude et al., 2013b; Vinken et al., 2014; Schreier et al., 2015; Cooper et al., 2017; Miyazaki et al., 2017; Liu et al., 2018). These observations have also been often used to assess chemical mechanisms (e.g., Martin et al., 2002; van Noije et al., 2006; Lamsal et al., 2008; Kim et al., 2009; Herron-Thorpe et al., 2010; Huijnen et al., 2010) and to infer the lifetime of NO_x (e.g., Schaub et al., 2007; Lamsal et al., 2010; Beirle et al., 2011) in chemical transport models (CTMs). Surface NO_2 concentrations (Lamsal et al., 2008, 2014; Novotny et al., 2011; Bechle et al., 2013) and NO_x deposition flux (Nowlan et al., 2014; Geddes and Martin, 2017) can also be estimated using satellite NO_2 observations. As the accuracy of any application of satellite data largely depends on the data quality, validation of satellite NO_2 observations is necessary.

A number of validation studies of space-based tropospheric NO_2 columns have been conducted using independent NO_2 observations from airborne in situ mixing ratio measurements (e.g., Boersma et al., 2008; Bucsela et al., 2008; Hains et al., 2010; Lamsal et al., 2014), ground-based total column (e.g., Pandora instrument; Herman et al., 2009) and tropospheric (MAX-DOAS instrument; e.g., Vlemmix et al., 2010; Irie et al., 2012) column measurements, and airborne high-resolution differential optical absorption spectroscopy (DOAS) measurements (Lamsal et al., 2017; Nowlan et al., 2018). Most validation studies utilizing in situ and ground-based observations have reported that satellite measurements tend to underestimate tropospheric NO_2 columns, especially over highly polluted areas (e.g., Hains et al., 2010). Intrinsic limits of space-based measurements, however, pose a challenge in comparisons between satellite, in situ, and ground-based measurements due to differences in representativeness. As stated above, NO_2 usually exhibits very sharp spatial gradients (tens of meters to kilometers). In contrast, the spatial resolution of satellite measurements is too coarse (tens of kilometers) to capture the fine spatial features of tropospheric NO_2 abundance. Therefore, it is important to recognize and account for the spatial variability while comparing satellite data with ground-based and in situ observations.

While the intrinsic resolution of satellite observations cannot be altered, there are ways to improve the derived satellite data products. The fidelity of the retrieved NO_2 product is dependent on the assumptions (e.g., NO_2 vertical profile shape, surface reflectivity) made in the retrieval algorithm. Some of the input parameters are available at much coarser resolution than the spatial resolution of OMI, introducing spatially (e.g., rural-to-urban) varying retrieval biases. Several studies show that the use of high-resolution NO_2 profiles results in significant improvements in retrievals (e.g., Russell et al., 2012; Lin et al., 2014; Lamsal et al., 2014; McLinden et al., 2014; Laughner et al., 2016, 2019; Goldberg et al., 2017). Deficiencies in model distributions of NO_2 may be identified and improved through rigorous evaluation with independent data, such as the suite of data collected during the Deriving Information on Surface Conditions from Column and Vertically Resolved Observations Relevant to Air Quality (DISCOVER-AQ) campaign deployments.

In this paper, we use comprehensive, integrated datasets of NO_2 gathered from surface, aircraft, and space instruments during NASA DISCOVER-AQ and the NASA and National Institute of Environmental Research (NIER) Korea–United States Air Quality Study (KORUS-AQ) together with NO_2 model simulations to address questions regarding retrieval accuracy. We describe the datasets in Sect. 2.1 and the models in Sect. 2.2. As an example, we focus on the NASA Standard NO_2 Product from OMI onboard the Aura satellite and conduct retrieval studies using the algorithm as discussed in Sect. 2.3, but the approaches discussed here could be applied to similar products as well. Results are presented in Sect. 3.

Table 1. Campaign locations and time periods.

Campaign	Location	Time period	Flight days
DISCOVER-AQ	Baltimore, Maryland	June–July 2011	14
DISCOVER-AQ	San Joaquin Valley, California	January–February 2013	11
DISCOVER-AQ	Houston, Texas	September 2013	10
DISCOVER-AQ	Denver–Ft. Collins, Colorado	July–August 2014	15
KORUS-AQ	Republic of Korea (South Korea)	May–June 2016	22

2 Observations and chemical transport models

2.1 NO_2 observations during DISCOVER-AQ and KORUS-AQ field campaigns

DISCOVER-AQ (https://www-air.larc.nasa.gov/missions/discover-aq/, last access: 5 September 2019) and KORUS-AQ (https://www-air.larc.nasa.gov/missions/korus-aq/, last access: 5 September 2019) were field study programs that provided comprehensive, integrated datasets of airborne and surface observations relevant to the diagnosis of surface air quality conditions from space. DISCOVER-AQ was a part of the NASA Earth Venture program and conducted four field deployments in Maryland (MD), California (CA), Texas (TX), and Colorado (CO) that covered different seasons and pollution regimes. KORUS-AQ was an international cooperation field study program conducted in the Republic of Korea (South Korea), sponsored by NASA and the South Korean government through the NIER. Table 1 summarizes the campaign locations and periods for the two field campaigns.

The primary objectives of DISCOVER-AQ and KORUS-AQ included (1) exploring the relationship between air quality at the surface and the tropospheric columns that can be derived from satellite orbit, (2) examining the diurnal variation of these relationships, and (3) characterizing the scales of variability relevant to the model simulation and remote observation of air quality. To accomplish these objectives, an observing strategy was designed to carry out systematic and concurrent in situ and remote sensing observations from a network of ground sites and research aircraft. The payloads on research aircraft consisted of several in situ instruments that differed minimally between campaigns. Ground-based trace gas observations included in situ surface and remote sensing Pandora measurements (Herman et al., 2009).

Figure 1 illustrates a conceptual view of the instruments and their sampling methods with their areal coverage for NO_2 observations. While the aircraft (P-3B for DISCOVER-AQ and DC-8 for KORUS-AQ) make spirals (P-3B) or ascents and descents (DC-8) over the site, the onboard National Center for Atmospheric Research (NCAR) and thermal dissociation laser-induced florescence (TD-LIF) instruments measure in situ NO_2 profiles. The aircraft usually visit each site two to four times a day to observe the diurnal variations of the NO_2 profiles. The P-3B aircraft made spirals of ~ 4 km diameter, whereas the DC-8 ascents and descents covered 10–20 km. Consequently, the distance between the ground and aircraft locations was 0–5 km during the DISCOVER-AQ and 10–20 km during the KORUS-AQ campaign. Pandora and NO_2 ground monitor instruments are typically located at ground stations close to the aircraft profiles. Throughout the day, Pandora reports the total column NO_2 from direct-sun measurements, and the ground monitor reports the in situ surface NO_2 mixing ratio. Finally, OMI retrievals report a tropospheric column NO_2 once a day in the afternoon; the OMI pixel has a much larger ground footprint compared with the in situ and Pandora measurements. Table 2 lists the sites with ground-based NO_2 monitors used in this analysis, along with the type of instrument employed at each site and the numbers of aircraft profiles and Pandora measurements available from each site near the time of OMI overpass. Detailed data descriptions follow in this section.

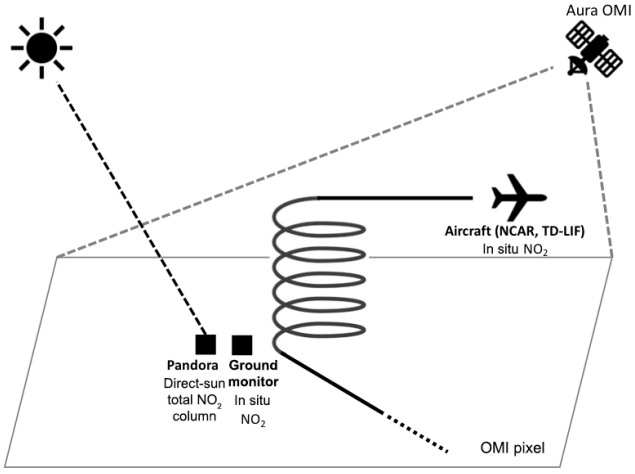

Figure 1. Conceptual illustration of NO_2 observations during the DISCOVER-AQ and KORUS-AQ field campaigns. The instruments used include ground-based monitors measuring in situ NO_2 volume mixing ratios, Pandora making direct-sun measurements to retrieve the total column NO_2, airborne instruments measuring in situ NO_2 profiles, and the Ozone Monitoring Instrument (OMI) aboard the Aura spacecraft reporting total column and tropospheric column NO_2.

Table 2. Summary of ground supersites during DISCOVER-AQ and KORUS-AQ campaigns with ground-based NO_2 measurements. The symbol *N* represents the sample size for aircraft and Pandora (in parentheses if different from that of aircraft profiles) measurements that are collocated with OMI observations. Surface NO_2 monitors include NO_x analyzers with molybdenum converters (MCs), NO_x analyzers with photolytic converters (PCs), cavity-attenuated phase shift (CAPS) spectrometers, and cavity ring-down spectrometers (CRDSs).

Campaign	Site	Latitude, longitude	Elevation (m)	*N*	Ground monitor type
MD	Padonia	39.46° N, 76.63° W	120	6 (4)	PC
	Fairhill	39.7° N, 76.86° W	109	3	PC
	Edgewood	39.4° N, 76.3° W	9	6 (5)	PC
	Essex	39.31° N, 76.47° W	13	3 (2)	MC
	Chesapeake[1]	39.16° N, 76.34° W[2]	–	3 (0)	–
CA	Bakersfield	35.33° N, 119.0° W	117	5 (3)	MC
	Porterville	36.03° N, 119.06° W	141	5	CAPS
	Hanford	36.32° N, 119.64° W	80	7 (6)	MC
	Fresno	36.79° N, 119.77° W	97	8	MC
TX	Galveston	29.25° N, 94.86° W	0	7	PC
	Manvel Croix	29.52° N, 95.39° W	18	6	CRDS
	Deer Park	29.67° N, 95.13° W	6	4	MC
	Moody Tower	29.72° N, 95.34° W	64	4 (2)	PC
	Channelview	29.80° N, 95.13° W	6	4	MC
	Conroe	30.35° N. 95.43° W	67	3	MC
CO	Fort Collins	40.59° N, 105.14° W	1577	3 (2)	MC
	Platteville	40.18° N, 104.73° W	1522.5	5 (4)	MC
	NREL-Golden	39.74° N, 105.18° W	1846	4 (2)	CAPS
	Bao Tower	40.04° N, 105.01° W	1590	4	CRDS
	Denver La Casa	39.78° N, 105.01° W	1602	5 (4)	MC
	Chatfield Park	39.53° N, 105.07° W	1675	5	MC
Korea	Olympic Park	37.52° N, 127.124°E	26	4 (3)	PC
	Taehwa	37.31° N, 127.311°E	160	7 (2)	CAPS

[1] Only aircraft spirals were performed over this site. [2] The coordinate is approximate.

2.1.1 Vertical distribution of NO_2 by aircraft

In situ NO_2 volume mixing ratios (VMRs) were measured from the NASA P-3B (DISCOVER-AQ) and DC-8 (KORUS-AQ) aircraft. The number of flights varied between campaigns, ranging from 10 for Texas to 22 for Korea. Flights took place during a range of conditions, e.g., pollution episodes, clean days, weekdays, and weekends. Measurements usually commenced in the morning and continued throughout the day with multiple sorties on a given day. During each sortie, the aircraft made vertical spirals over surface sites, sampling NO_2 between ~ 300 m and 5 km from the Earth's surface. In Maryland, spirals were also made over the Chesapeake Bay area, which did not have any ground monitors.

Airborne measurements were carried out using two different instruments and measurement techniques. The four-channel chemiluminescence instrument from the National Center for Atmospheric Research (NCAR) measured NO_2 by the photolysis of NO_2 and subsequent chemiluminescence detection of NO_2 following the oxidation of the photolysis product NO with ozone (Ridley and Grahek, 1990). This instrument has an NO_2 measurement uncertainty of 10 % and a 1 s, 2σ detection limit of 50 parts per trillion by volume (pptv). We hereafter refer to these NO_2 measurements as "NCAR". The thermal dissociation laser-induced florescence (TD-LIF) method used by the University of Berkeley detects NO_2 directly and other nitrogen species (e.g., total peroxynitrates, alkyl nitrates, HNO_3) following the thermal dissociation of all oxides of nitrogen (NO_y) to NO_2 (Thornton et al., 2000). The laser-induced fluorescence method is highly sensitive for measuring NO_2, with a detection limit of 30 pptv. The measurement uncertainty is 5 %. This instrument has a lower NO_2 sampling frequency than the NCAR instrument due to its alternating measurement cycle for different species. We refer to these NO_2 measurements as TD-LIF.

Here we use 1 s merged data provided in the campaign data archives and focus on early afternoon measurements made within 1.5 h of the OMI overpass time (13:45 approximately). This time window of ± 1.5 h is selected to maximize the number of samples while reducing effects from the diurnal variation of NO_2. Figure 2 shows the mean NO_2 profile for each of the DISCOVER-AQ and KORUS-AQ campaigns. Measurements show considerable spatiotemporal variation

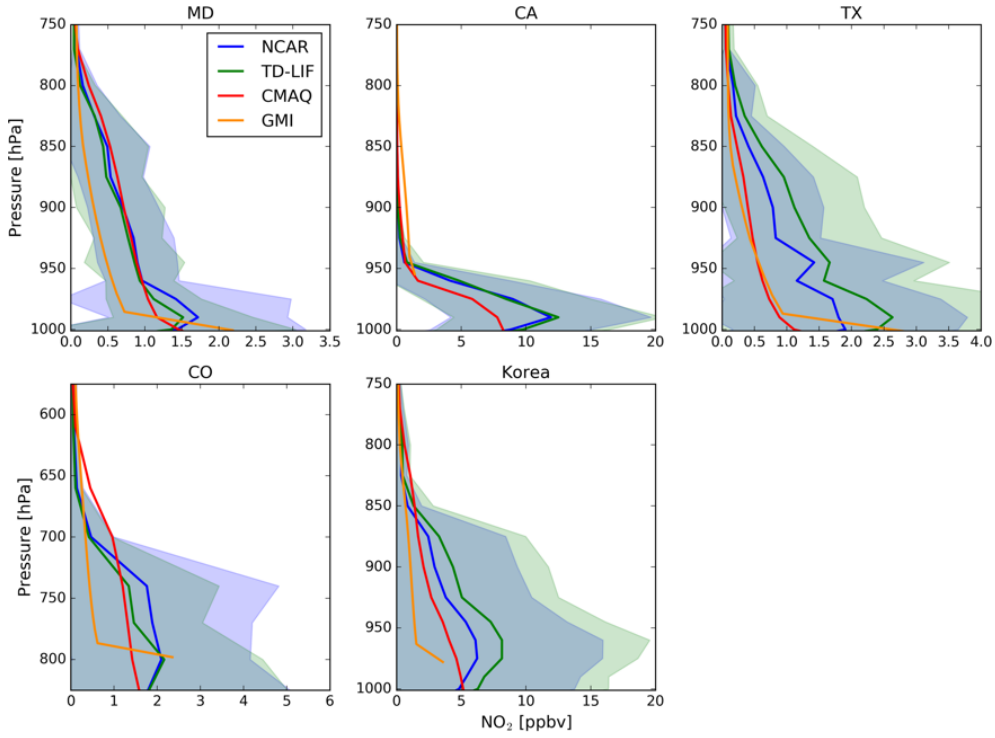

Figure 2. Mean early afternoon NO_2 profiles, both observed and modeled, for the DISCOVER-AQ and KORUS-AQ campaigns. Colored lines represent the average for airborne in situ profiles from NCAR (blue) and TD-LIF (green) instruments compared with simulated profiles from the GMI global model (orange) and the CMAQ (DISCOVER-AQ) or WRF-Chem (KORUS-AQ) regional models (red). The standard deviations of airborne profiles are indicated as shaded areas for NCAR (lavender) and TD-LIF (green) instruments. The blue–gray color represents the overlap of the two.

as well as some indication of a well-developed mixing layer, with the maximum mixing ratio near the ground. The mixing layer heights vary by region and season. For example, in the MD campaign conducted in summer, the mixing layer stretches up to 800 hPa (2 km). In contrast, the mean profiles from the CA campaign conducted in winter show a shallow mixing layer extending only up to 950 hPa ($\sim$ 700 m). Near-surface NO_2 mixing ratios also vary by campaign location and possibly by season, with the highest near-surface NO_2 in CA. In South Korea, the mean near-surface NO_2 mixing ratio is not as high as in CA, but a very high ($\sim$ 5 ppbv) NO_2 mixing ratio stretches up to 850 hPa, resulting in the greatest NO_2 column. While the NCAR and TD-LIF mean profiles generally agree with each other in the MD, CA, and CO campaigns, they exhibit larger differences in TX and South Korea. Figure 2 also shows the nature of the variability in observed and simulated NO_2 vertical profiles over the campaign domains. The observed differences between the model and observations arise primarily from a mismatch in both spatial and temporal sampling. The use of more restrictive collocation (spatial and temporal) applied for comparing different datasets in Sect. 3.1 and examining the air mass factor (AMF) effect in Sect. 2.3.2 would have resulted in different vertical distributions.

2.1.2 In situ surface NO_2 measurements

To extend the altitude range of the vertical profiles discussed in Sect. 2.1.1, we merge in situ aircraft profile measurements with coincident in situ surface NO_2 measurements sampled over the duration of spirals ($\sim$ 20 min) by linearly interpolating the NO_2 mixing ratios between the surface and the lowest aircraft altitudes. These new merged profiles contain a greater portion of the tropospheric NO_2 column. During both the DISCOVER-AQ and KORUS-AQ campaigns, in situ surface NO_2 monitors were deployed at several ground sites (Table 2). Measurements were carried out using one of four different types of NO_2 monitors, including a chemiluminescence NO_x monitor equipped with either a molybdenum or photolytic converter, a cavity-attenuated phase shift (CAPS) spectrometer, and a cavity ring-down spectrometer (CRDS). The molybdenum converter analyzer measures NO_2 indirectly by the thermal conversion of NO_2 to NO using molybdenum and the detection of NO by chemiluminescence that results from the reaction of NO with ozone. Since the reduction process could convert not only NO_2 but also other reactive nitrogen species, this instrument could overestimate NO_2 concentrations (Dunlea et al., 2007; Steinbacher et al., 2007; Lamsal et al., 2008; Dickerson et al., 2019). The mag-

nitude of interference depends on the relative concentrations of NO_2, nitric acid, alkyl nitrates, and peroxy-acetyl nitrate, which vary spatially, diurnally, and seasonally and are difficult to quantify. Considering their use in the sections below (Sects. 2.3.2 and 3), we conducted a sensitivity study examining how 0 %–50 % biases in molybdenum converter measurements could impact tropospheric columns derived from merged (aircraft + surface) profiles. We found that the errors are usually rather small at $< 6\,\%$ for various sites. Therefore, no attempt is made here to correct for the interference in these measurements, although we identify those sites in Table 2 and Fig. 6.

The operating principle of a photolytic converter analyzer is also gas-phase chemiluminescence, but the use of a photolytic converter to reduce NO_2 to NO makes it more specific to NO_2. As a result, this instrument provides nearly interference-free NO_2 measurements, with the exception of nitrous acid (HONO; Ryerson et al., 2000). Measurement uncertainties for 1 h averages are expected to be $\sim 10\,\%$ (Fehsenfeld et al., 1990).

The CAPS instrument detects NO_2 by measuring absorption around 450 nm. Baseline measurements spanning minutes to hours with a source of NO_2-free air are needed to determine NO_2 amounts. In contrast to the chemiluminescence–molybdenum converter techniques, CAPS directly detects NO_2. Its specificity for NO_2 is affected by potential interference from species like glyoxal, water vapor, and ozone that absorb light within the band pass of the instrument. The detection limit is < 0.1 ppb for a 10 s measurement. NO_2 measurements from CAPS and chemiluminescence NO_x monitors with a molybdenum converter are reported to agree to within 2 % (Kebabian et al., 2008).

A CRDS is a sensitive and compact detector that measures multiple nitrogen species including NO_2. It employs a laser diode at 405 nm for the direct detection of NO_2. Interferences arising from absorption by other trace gases, such as ozone and water vapor, are expected to be small. The measurement precision is 20 ppt at a 1 s time resolution and the accuracy is better than 5 %, which is primarily limited by the NO_2 absorption cross section used in the data reduction process. The total reactive nitrogen (NO_y) measured by the CRDS and chemiluminescence NO_x monitor with a molybdenum converter is found to agree to within 12 % (Wild et al., 2014).

2.1.3 Pandora total column NO_2

In addition to in situ measurements, each campaign hosted ground-based networks of Pandora instruments. Pandora is a small, commercially available sun-viewing spectrometer optimized for the detection of trace gases, including NO_2. It measures direct solar spectra in the 280–525 nm spectral range with 0.6 nm resolution. A detailed description of the instrument's design, operation, and retrieval method can be found in Herman et al. (2009, 2018). The NO_2 retrieval algorithm includes (1) a direct-sun spectral fitting method similar to traditional differential optical absorption spectroscopy (DOAS) (Platt, 1994) using one measurement (or an average of several measurements) as a reference spectrum to derive relative NO_2 slant column densities (SCDs), (2) the application of the Modified Langley Extrapolation (MLE) to derive total NO_2 SCDs, and (3) the conversion of total NO_2 SCDs to vertical column densities (VCDs) using the direct-sun air mass factor (AMF) as follows:

$$\mathrm{VCD} = \mathrm{SCD}/\mathrm{AMF}. \tag{1}$$

The spectral fitting is performed over the 400–440 nm window; it fits NO_2 cross sections at 254.5 K (Vandaele et al., 1998), ozone (Brion et al., 1993), and a fourth-order smoothing polynomial, and it applies a wavelength shift and a constant offset. In clear-sky conditions, this instrument provides total NO_2 VCD with a precision of 2.7×10^{14} and an absolute accuracy of 1.3×10^{15} molec cm^{-2} (Herman et al., 2018). Potential sources of error in NO_2 retrievals include the calibration of raw data, the chosen reference spectrum, and the use of a fixed temperature for the NO_2 cross section. Pandora NO_2 data have been compared with data from direct-sun multifunction DOAS (MFDOAS) and Fourier transform ultraviolet spectrometry (UVFTS) (Herman et al., 2009) and have been found to agree within 12 %. These data are regularly used to validate satellite NO_2 retrievals (e.g., Lamsal et al., 2014; Tzortziou et al., 2015, 2018; Ialongo et al., 2016).

Here, we use clear-sky quality-controlled (root mean square (rms) < 0.05 and errors < 0.05 DU) 80 s total column NO_2 data averaged over the duration of each aircraft spiral. We infer tropospheric column NO_2 by subtracting the OMI stratospheric column from the Pandora total column to compare with tropospheric NO_2 from in situ and OMI observations.

2.2 NO_2 simulations

2.2.1 GMI simulation

The Global Modeling Initiative (GMI) three-dimensional chemical transport model (CTM) simulates the troposphere and stratosphere (Strahan et al., 2013) with a stratosphere–troposphere chemical mechanism (Duncan et al., 2007) updated with the latest chemical rate coefficients (Burkholder et al., 2015) and time-dependent natural and anthropogenic emissions (Strode et al., 2015). Aerosol fields are computed online with the Goddard Chemistry Aerosol Radiation and Transport (GOCART) model (Chin et al., 2014, and references therein). Tropospheric processes such as NO_x production by lightning, scavenging, and wet and dry deposition are also represented in the model. The GMI simulations used in this work were constrained with meteorology from the Modern-Era Retrospective Analysis for Research and Applications version 2 (MERRA-2) meteorolog-

ical fields (Gelaro et al., 2017) at 72 vertical levels from the surface to 0.01 hPa, with a resolution ranging from ~ 150 m in the boundary layer to ~ 1 km in the upper troposphere and lower stratosphere, and at a horizontal spatial resolution of 1.25° longitude $\times$ 1.0° latitude.

GMI simulations have been evaluated in the troposphere and stratosphere. Strode et al. (2015) showed good agreement with tropospheric O_3 and NO_x trends in the US in a 1990–2013 hindcast simulation. Strahan et al. (2016) demonstrated realistic seasonal and interannual variability of Arctic composition using comparisons to Aura MLS O_3 and N_2O. The simulation of NO_2 in both the troposphere (Lamsal et al., 2014) and stratosphere (Spinei et al., 2014; Marchenko et al., 2015) has been shown to be in good agreement with independent measurements. We sample the model profile at the times and locations of airborne measurements. Figure 2 compares GMI NO_2 profiles with collocated aircraft measurements during the DISCOVER-AQ and KORUS-AQ field campaigns. The GMI simulation generally captures the vertical distribution of NO_2 in the free troposphere, is somewhat lower in the middle and upper parts of the mixing layer, and exhibits sharper gradients between the boundary layer and the surface. Due to the coarse spatial resolution of the GMI model, the surface pressure of the GMI profiles differs from the measurements, especially over complex terrain in CA, CO, and Korea.

2.2.2 NO_2 simulations using regional models

For each DISCOVER-AQ and KORUS-AQ deployment, a high-resolution model simulation was conducted. We use NO_2 profiles from those simulations to examine their effect on retrievals in Sect. 2.3.2 and to downscale OMI NO_2 retrievals in Sect. 2.3.3. Below we provide a brief description of each simulation. Information about model options for these simulations can be found in Table A1 in the Appendix. For most of the campaigns, the near-surface NO_2 concentration and the model profile shapes agree in general with the NCAR and TD-LIF profiles. In TX, however, the CMAQ simulation shows lower mixing ratios than observations throughout the mixing layer (Fig. 2).

MD. The Weather Research and Forecasting (WRF) model was run (Loughner et al., 2014) from 24 May through 1 August 2011 at horizontal resolutions of 36, 12, 4, and 1.33 km with 45 vertical levels from the surface to 100 hPa with 16 levels within the lowest 2 km. Meteorological initial and boundary conditions were taken from the 12 km North American Mesoscale (NAM) model. Output from the 4 and 1.33 km WRF simulations were fed into the Community Multiscale Air Quality (CMAQ; Byun and Schere, 2005). Chemical initial and boundary conditions for the 4 km CMAQ run came from a 12 km CMAQ simulation covering the continental US, which was performed for the GEO-CAPE Regional Observing System Simulation Experiment (OSSE). The creation of the emissions used within the CMAQ simulation is described in Loughner et al. (2014) and Anderson et al. (2014). CMAQ was run with reduced mobile emissions by 50 % and an increase in the photolysis frequency of organic nitrate species based on Anderson et al. (2014).

CA. The coupled WRF–CMAQ modeling system (Wong et al., 2012) was run from 1 January through 28 February 2013 (2013 DISCOVER-AQ California campaign period) at horizontal resolutions of 4 and 2 km, with 35 vertical levels from the surface to 50 hPa and an average height of the middle of the lowest layer of 20 m. WRF version 3.8 and CMAQ version 5.2.1 were used in a coupled format, allowing for frequent communication between the meteorological and chemical transport models and indirect effects from aerosol loading on the meteorological calculations in WRF. Meteorological initial and boundary conditions were taken from the 12 km NAM reanalysis product from NOAA statistical and mathematical symbols. Observation nudging above the planetary boundary layer (PBL) using four-dimensional data assimilation (FDDA) was applied in WRF. Chemical initial and boundary conditions for the 4 km CMAQ simulation came from a 12 km CMAQ simulation covering the continental US, while initial and boundary conditions for the 2 km simulation were obtained from the 4 km WRF–CMAQ simulation. Emissions are based on the 2011 US National Emissions Inventory (NEI) with year-specific updates to point and mobile sources, while biogenic emissions were calculated inline in CMAQ using the Biogenic Emissions Inventory System (BEIS).

TX. To simulate the DISCOVER-AQ Texas campaign, a WRF model simulation was performed from 18 August through 1 October 2013, covering the entire field deployment in September 2013. The model was run at 36, 12, 4, and 1.33 km horizontal resolutions with 45 levels from the surface to 50 hPa. Meteorological initial and boundary conditions were taken from the 12 km North American Mesoscale (NAM) model. Output from the 4 and 1.33 km simulations were used to run the CMAQ model. Chemical and initial boundary conditions for the outer domain were taken from the Model for Ozone and Related chemical Tracers (MOZART) chemical transport model (CTM). Detailed information about these simulations and the emissions used can be found at http://aqrp.ceer.utexas.edu/projectinfoFY14_15/14-004/14-004FinalReport.pdf (last access: 5 September 2019).

CO. For the Colorado deployment, WRF was run from 9 July through 20 August 2014 at spatial resolutions of 12 km (covering the western US) and 4 km (covering Colorado). The model top was set at 50 hPa, with 37 levels in the vertical. Analysis fields from the European Centre for Medium-Range Weather Forecasts (ECMWF) were used for meteorological initial and boundary conditions. Chemical initial and boundary conditions for the outer domain were taken from Real Time Air Quality Monitoring System (RAQMS) model output. Further information about

this simulation can be found at https://www.colorado.gov/airquality/tech_doc_repository.aspx?action=open&file=FRAPPE-NCAR_Final_Report_July2017.pdf (last access: 5 September 2019).

Korea. Air quality forecasts were performed using the Weather Research and Forecasting model (Skamarock et al., 2008) coupled to the Chemistry (WRF-Chem) (Grell et al., 2005) model to support KORUS-AQ flight planning and post-campaign analysis. The modeling domains consist of a regional domain of 20 km resolution covering major sources of transboundary pollutants affecting the Korean Peninsula: anthropogenic pollution from eastern China, dust from inner China and Mongolia, and wildfires from Siberia (Saide et al., 2014). A 4 km resolution domain was nested and covered the Korean Peninsula and surroundings, which encompassed the region where the DC-8 flights were planned and better resolved local sources. Anthropogenic emissions were developed by Konkuk University for KORUS-AQ forecasting and are described in Goldberg et al. (2019).

2.3 OMI NO_2 observations

The Ozone Monitoring Instrument (OMI) aboard the NASA Aura satellite provides measurements of solar backscatter that are used to retrieve total, stratospheric, and tropospheric NO_2 columns with a native ground resolution varying from 13 km × 24 km near nadir to 40 km × 250 km at swath edges (Levelt et al., 2006, 2018). The Aura satellite was launched on 15 July 2004 into a sun-synchronous polar orbit with a local Equator crossing time of 13:45 in the ascending node. OMI is one of the most stable UV–Vis satellite instruments providing a long-term high-resolution data record with low degradation (Dobber et al., 2008; DeLand and Marchenko, 2013; Schenkeveld et al., 2017). In the middle of 2007, an anomaly began to appear in OMI radiances in certain rows affecting all Level 2 products (Schenkeveld et al., 2017). This "row anomaly" can be easily identified, and the affected rows are discarded. We use OMI pixels with a cloud radiance fraction less than 50 % and quality flags indicating good data.

2.3.1 Standard OMI NO_2 Product

Here we use the Standard OMI NO_2 Product (OMNO2) version 3.1, with updates from version 3.0 (Krotkov et al., 2017). The NO_2 retrieval algorithm uses the differential optical absorption spectroscopy (DOAS) technique. The retrieval method includes (1) the determination of NO_2 slant column density (SCD) using a DOAS spectral fit of the NO_2 cross section from measured reflectance spectra over the 402–465 nm range; (2) the calculation of an air mass factor (AMF) that is required to convert SCD into vertical column density (VCD); and (3) a scheme to separate stratospheric and tropospheric VCDs. The AMF calculation is performed by combining NO_2 measurement sensitivity (scattering weights) from the TOMS RADiative transfer model (TOMRAD; Dave, 1964) with the a priori relative vertical distribution (profile shape) of NO_2 taken from the GMI CTM. Computation of scattering weights requires information on viewing and solar geometries, terrain and cloud reflectivities, terrain and cloud pressures, and cloud cover (radiative cloud fraction).

The version used here represents a significant advance over previous versions (Bucsela et al., 2006, 2013; Celarier et al., 2008; Lamsal et al., 2014). It includes an improved DOAS algorithm for retrieving slant column densities (SCDs) as discussed in Marchenko et al. (2015). The key features of the algorithm include more accurate wavelength registration between Earth radiance and solar irradiance spectra, iterative accounting of the rotational Raman scattering effect, and sequential SCD retrieval of NO_2 and interfering species (water vapor and glyoxal). Solar irradiance reference spectra are monthly average data derived from OMI measurements instead of an OMI composite solar spectrum used in prior versions. Cloud pressure and cloud fraction are taken from an updated version of the OMCLDO2 cloud product that includes updated lookup tables and O_2–O_2 SCD retrieved with a temperature correction (Veefkind et al., 2016). A priori NO_2 profiles are as discussed in Lamsal et al. (2015) and Krotkov et al. (2017) and use 1° latitude × 1.25° longitude GMI model-based monthly a priori NO_2 profiles with year-specific emissions. This retrieval version also uses more accurate information on terrain pressure that is calculated from high-resolution digital elevation model (DEM) data at 3 km resolution and GMI terrain pressure.

2.3.2 Recalculation of OMI NO_2 AMF using alternative NO_2 profiles

NO_2 vertical profiles, especially in the troposphere, vary strongly in both space and time. The simulated NO_2 profiles from a global CTM (GMI) employed in the operational NO_2 retrieval, while offering a good option at a global scale, may not sufficiently capture the distribution of NO_2 at OMI's ground resolution. Using precalculated scattering weights (Sw) made available in the OMNO2 product and alternative information on vertical NO_2 profile shape (Xa), the OMI NO_2 AMF can be readily recalculated (Lamsal et al., 2014):

$$\mathrm{AMF_{trop}} = \frac{\sum_{\mathrm{surface}}^{\mathrm{tropopause}} \mathrm{Sw} \cdot \mathrm{Xa}}{\sum_{\mathrm{surface}}^{\mathrm{tropopause}} \mathrm{Xa}}, \tag{2}$$

where the integral from the surface to the tropopause yields the tropospheric AMF ($\mathrm{AMF_{trop}}$). Scattering weights vary with viewing and solar geometry, cloud–aerosol conditions, and surface reflectivity, but they are assumed to be independent of the vertical distribution of NO_2. The typical vertical distribution of scattering weights is characterized by lower values in the troposphere due to reduced sensitivity owing to Rayleigh scattering and higher values (corresponding to a nearly geometric AMF) in the stratosphere. The AMF is

therefore highly sensitive to NO_2 profile shape in the lower troposphere.

Here, we investigate how a priori NO_2 profiles affect OMI tropospheric AMF and consequently the retrieval of OMI tropospheric NO_2 VCD. For this, we combine the measured profile (from the surface to ~ 5 km) with coincidently sampled simulated NO_2 from GMI (5 km to the tropopause) to create a complete tropospheric NO_2 profile. We choose the GMI simulation over the high-resolution model simulations because we found that the GMI generally better performed in the free troposphere compared to the regional models. We then interpolate the pressure-tagged NO_2 observations (aircraft NCAR NO_2 + surface) onto the pressure grid of the OMI NO_2 scattering weight. The tropospheric AMFs obtained using individual measured profiles (AMF_{obs}) are compared with the AMFs in the OMI Standard Product (AMF_{SP}), which are calculated using the GMI yearly varying monthly climatology (Fig. 3a). AMF_{SP} is generally higher than AMF_{obs} by 34 % on average, with the largest difference (61.6 %) for TX and the smallest difference (16.6 %) for Korea; this means that the OMI SP VCDs, based on the AMF_{SP}, are correspondingly smaller on average than the those based on measured profiles. The correlation ranges from fair ($r = 0.41$, $N = 21$) for MD and TX to excellent ($r \geq 0.92$, $N = 36$) for CA and Korea, with the overall correlation coefficient of 0.53.

To explore how NO_2 profiles from high-resolution model simulations could affect OMI NO_2 retrievals, we calculate tropospheric AMFs using simulated monthly NO_2 profiles (AMF_{HR}). Since the OMI ground pixel size is much larger than the model grid boxes, we derive an average profile of all model grid boxes located within one OMI pixel and use it to calculate AMF_{HR}. Figure 3b compares AMF_{obs} with AMF_{HR}; it suggests improved agreement compared to AMF_{SP} (Fig. 3a), especially for CA, CO, and Korea, although with no significant improvement in the correlation.

We also considered how using AMFs based on monthly mean profiles, such as the OMI SP, impacts retrieved NO_2. To assess this, we calculated AMFs using both daily (AMF_{obs}) and campaign-average measured NO_2 profiles ($AMF_{obs\text{-}m}$). Figure 3c shows that AMF_{obs} and $AMF_{obs\text{-}m}$ agree to within 5.3 % and exhibit excellent correlation ($r > 0.8$). That is, the use of a mean profile does not make a significant difference compared to the individual daily profiles, implying that the average profile generally captures the local vertical distribution fairly well. Somewhat larger scatter in TX may be related to stronger land–sea breeze dynamics that could affect the vertical distribution of NO_2 in both the boundary layer and free troposphere. Our results here differ from previous studies that reported improved agreement of OMI NO_2 retrievals using simulated daily NO_2 profiles with independent observations (Valin et al., 2013; Laughner et al., 2019), although Laughner et al. (2019) also suggested poorer performance with daily profiles in the southeast US than in other regions.

2.3.3 Downscaled OMI NO_2 data

The NO_2 value associated with an OMI ground pixel is averaged over a large area. This spatial smoothing leads to a loss of information on sub-pixel variation, which could be considerable for NO_2, especially over urban source regions. Therefore, it is important to recognize and address this limitation while assessing, interpreting, and using satellite NO_2 data. Here we use high-resolution NO_2 model simulations for sub-pixel variation.

We apply the method described by Kim et al. (2016, 2018) to downscale OMI NO_2 retrievals, which are then compared with aircraft and Pandora data. This method applies high-resolution model-derived spatial-weighting kernels to individual OMI pixels and calculates sub-pixel variability within the pixel. The major assumption is that the model captures the spatial distribution of emission sources and NO_2 transport patterns well. The method ensures that the quantity (total number of molecules) of the satellite data over the pixel is numerically preserved, while adding higher-resolution spatial information to the derived tropospheric NO_2 columns.

Figure 4 illustrates the downscaling of tropospheric NO_2 for an OMI pixel using the high-resolution CMAQ simulation over Essex, Maryland. The tropospheric NO_2 column observed by OMI (5.9×10^{15} molec cm^{-2}) is 25.7 % higher than the average of the CMAQ NO_2 columns over the pixel. The spatial-weighting kernels suggest more than an order of magnitude difference in NO_2 within this single OMI pixel. Applying the kernels to the original OMI pixel value results in a range of sub-pixel NO_2 column values from 1.9×10^{15} over a clean background to 3.2×10^{16} molec cm^{-2} over a polluted hot spot.

Figure 5 demonstrates how the downscaled OMI NO_2 data using high-resolution NO_2 output from a CMAQ simulation compare with the original OMI NO_2 data from the standard product. Both OMI SP and CMAQ show enhanced NO_2 columns at major urban areas, but their magnitudes differ, with OMI showing lower values. As described above, OMI's field of view covers a large area, sampling the NO_2 field over the entire pixel, while the actual NO_2 distribution (better resolved by the CMAQ simulation) is defined by local source strengths, chemistry, and wind patterns that can occur at much finer spatial scales. By employing the relative ratios inside an OMI pixel rather than the overall magnitude of simulated columns, the downscaling technique yields a more detailed structure, enhancing NO_2 over sources and dampening it elsewhere by more than a factor of 2.

3 Results and discussion

3.1 Comparison between in situ observations

Figure 6a and Table 3 summarize how the two airborne in situ NO_2 tropospheric column measurements compare. We

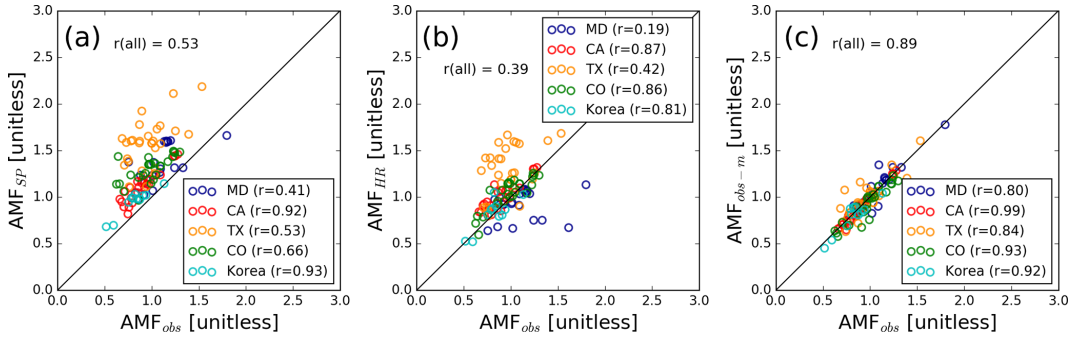

Figure 3. Comparison of AMFs calculated using observed NO_2 profiles (AMF_{obs}) with tropospheric AMFs in the OMI Standard Product (AMF_{SP}, **a**), and those calculated using NO_2 profiles from high-resolution model simulations (AMF_{HR}, **b**). Panel **(c)** compares tropospheric AMFs using daily versus campaign-average profiles ($AMF_{obs\text{-}m}$). The symbols are color-coded by campaign location.

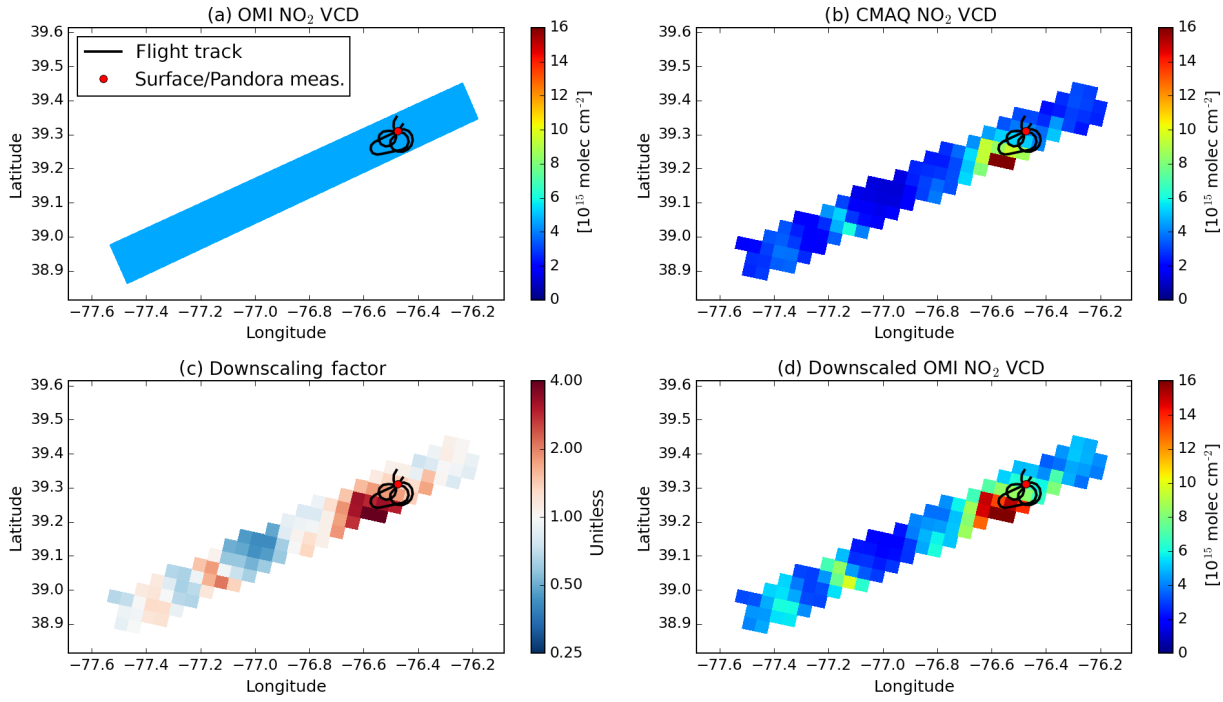

Figure 4. An illustration of downscaled OMI NO_2 for an OMI pixel over Essex, MD, from orbit 37024 on 1 July 2011. Shown are the original OMI tropospheric NO_2 VCD **(a)**, coincidently sampled CMAQ NO_2 VCD at a spatial resolution of $4 \times 4\,km^2$ **(b)**, the spatial-weighting kernel **(c)**, and downscaled OMI tropospheric NO_2 VCD **(d)**. These pixels coincide with an airborne in situ NO_2 profile sampled during the DISCOVER-AQ Maryland campaign, and the flight route is marked with a black line. The location of the NO_2 surface monitor and Pandora instrument is marked with a red dot.

derive the column amount by first extending the NCAR and TD-LIF NO_2 profiles to the same surface NO_2 concentration measurements and then integrating the NO_2 profiles. The only exception is at the Chesapeake Bay during the MD campaign, the only marine site used in this study; we extend a constant NO_2 mixing ratio measured at the lowest aircraft altitudes to the surface. To compare with OMI and Pandora retrievals, NO_2 amounts for the missing portion from the top of the aircraft altitude to the tropopause are added from the GMI simulation. This amount varied between 4.7×10^{14} and 1.2×10^{15} molec cm^{-2} and represented an average 5 % of the tropospheric NO_2 columns but can reach up to 50.8 % for an individual profile. Overall, the two airborne in situ columns generally agree very well and exhibit excellent correlation ($r = 0.87$–0.99). The correlation and mean difference differ among the five campaigns, with TD-LIF higher than NCAR by 31.9 % in TX and 11.6 % in Korea but lower by ~ 10 % in MD and CO. The observed difference in TX is much larger than the reported uncertainty of both NCAR and TD-LIF measurements. Analysis of individual profiles suggests that

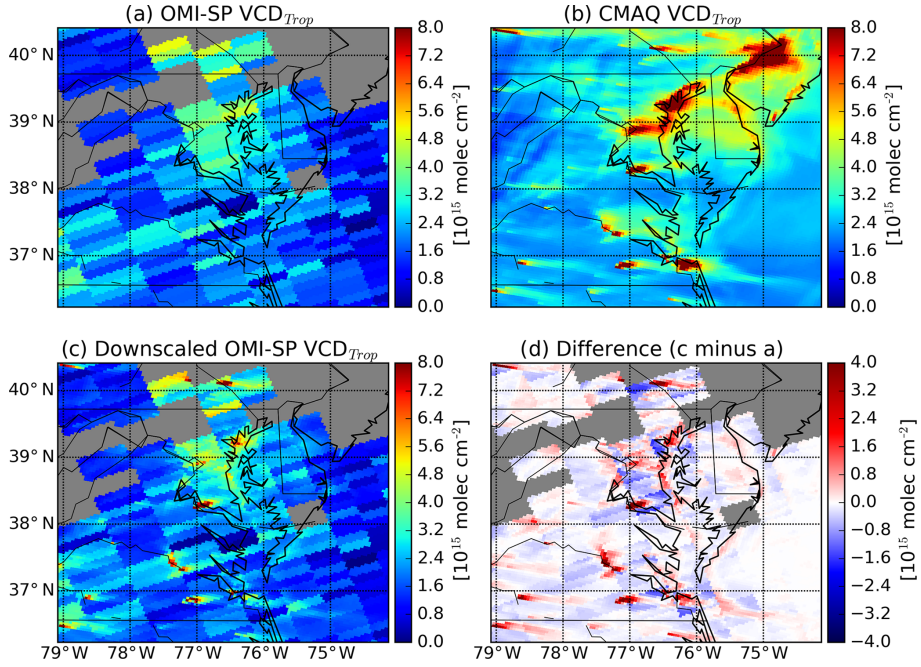

Figure 5. Tropospheric NO_2 VCD maps from **(a)** OMI SP, **(b)** CMAQ, and **(c)** downscaled OMI over Maryland on 29 July 2011. Panel **(d)** shows the difference between downscaled and standard tropospheric NO_2 VCD data (c minus a). The gray areas represent pixels with an effective cloud fraction > 0.3.

Table 3. Comparison between NCAR, TD-LIF, and Pandora NO_2 observations.

Campaign	NCAR vs. TD-LIF		NCAR vs. Pandora		TD-LIF vs. Pandora	
No. of profs. (Pandora)	Mean diff. (%) (TD-LIF – NCAR)	r	Mean diff. (%) (Pandora – NCAR)	r	Mean diff. (%) (Pandora – TD-LIF)	r
MD 21 (14)	−9.6	0.87	−24.5	0.42	−18.3	0.18
CA 25 (22)	7.2	0.93	11.1	0.65	4.8	0.58
TX 28 (26)	31.9	0.97	−39.1	0.94	−53.9	0.93
CO 26 (21)	−6.6	0.99	−2.8	0.81	4.2	0.78
Korea 11 (5)	11.6	0.99	20.3	0.95	7.5	0.94
All 111 (88)	8.3	0.99	−2.0	0.92	−9.8	0.90

the data from TD-LIF are generally higher than NCAR at all altitudes, regardless of the NO_2 pollution level (Fig. 7). The underlying cause of this difference is not clear, but it may be associated with the applied calibration standard or an interference issue for either or both of the two measurements. The small difference elsewhere could come from the lower measurement frequency of TD-LIF compared with the NCAR instrument.

3.2 Comparison between Pandora and aircraft observations

Figure 6b–c and Table 3 show the comparison between Pandora and the two airborne tropospheric NO_2 column measurements. We derive tropospheric columns from Pandora by subtracting collocated OMI stratospheric NO_2 columns from the Pandora total column NO_2 retrievals. The relationship between the aircraft and Pandora data is not as good as between the two aircraft measurements themselves. The use of OMI stratospheric NO_2 columns to derive tropospheric columns from Pandora could impact the comparison between Pandora and aircraft observations; this approach is unlikely to be a significant factor over the polluted DISCOVER-AQ and KORUS-AQ campaign domains. The correlation ranges from fair ($r = 0.42$) to excellent ($r = 0.95$) for NCAR versus Pandora and poor ($r = 0.18$) to excellent ($r = 0.94$) for TD-LIF versus Pandora. The overall correlation coefficients between Pandora and the airborne NCAR and TD-LIF measurements are 0.94 and 0.91, respectively, with higher correlation in CO, TX, and Korea and lower correlation in MD and CA. Pandora data are about a factor of 2 lower than air-

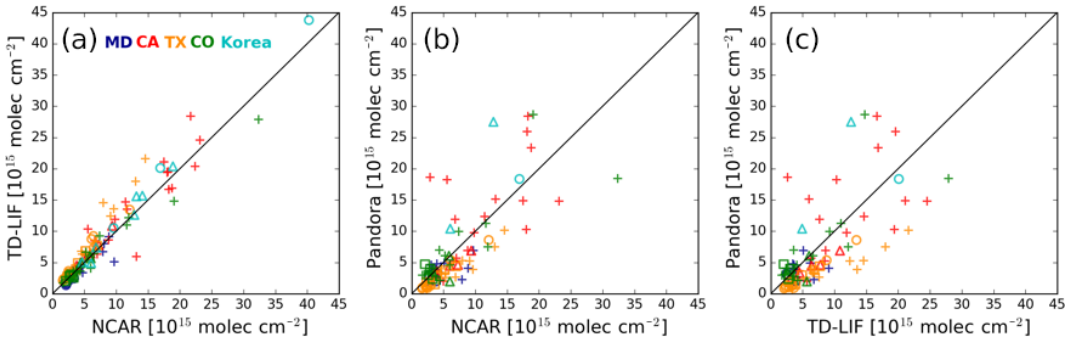

Figure 6. Comparison of NO_2 tropospheric columns derived from NCAR, TD-LIF, and Pandora instruments. Different colors represent the campaign location, and the symbols represent the type of surface monitor (open circle: photolytic converter, plus: molybdenum converter, triangle: CAPS, square: CRDS).

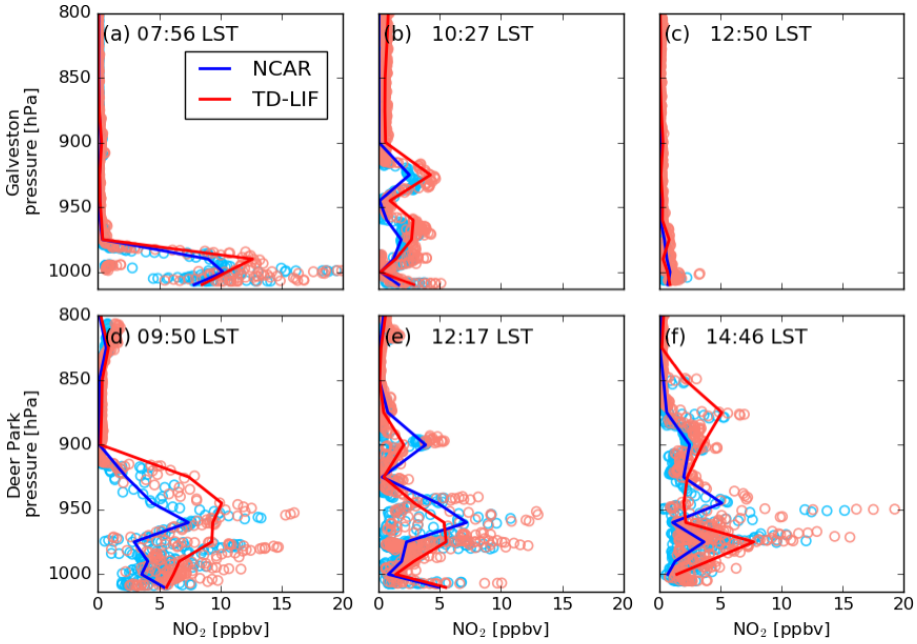

Figure 7. Vertical distribution of NO_2 mixing ratios at different local solar time (LST) over Galveston **(a, b, c)** and Deer Park **(d, e, f)** in TX measured by the NCAR (light blue) and TD-LIF (orange) instruments. The circles in lighter colors represent 1 s measurements, and the solid lines show the mean values for NCAR (blue) and TD-LIF (red).

craft measurements in TX. Elsewhere, Pandora data agree with aircraft measurements to within 20 % on average, although much larger differences are observed for individual sites. A larger discrepancy for Pandora data in TX is also reported by Nowlan et al. (2018), who used various NO_2 measurements to evaluate GeoTASO NO_2 retrievals. The reasons for such exceptionally large differences could include strong gradients in the NO_2 field that are missed by aircraft spirals, errors in Pandora retrievals, or both.

3.3 Assessment of OMI NO_2 retrievals

We compare OMI tropospheric NO_2 columns with Pandora data and vertically integrated columns from aircraft spirals at 23 locations (Table 2) during the DISCOVER-AQ and KORUS-AQ field campaigns. We only analyze OMI pixels that overlap individual aircraft profiles. Spatially collocated aircraft and Pandora data are temporally matched to OMI by allowing only the measurements made within 1.5 h of the OMI overpass time. We infer tropospheric columns from Pandora by subtracting OMI-derived stratospheric NO_2 from Pandora total columns.

Figure 8a and b and Table A2 present tropospheric NO_2 columns from the OMI Standard Product compared with integrated columns from the NCAR and TD-LIF instruments. Although the OMI and aircraft data are significantly correlated ($r = 0.39$–0.87), OMI NO_2 retrievals are generally lower, with the largest difference in CO and the smallest dif-

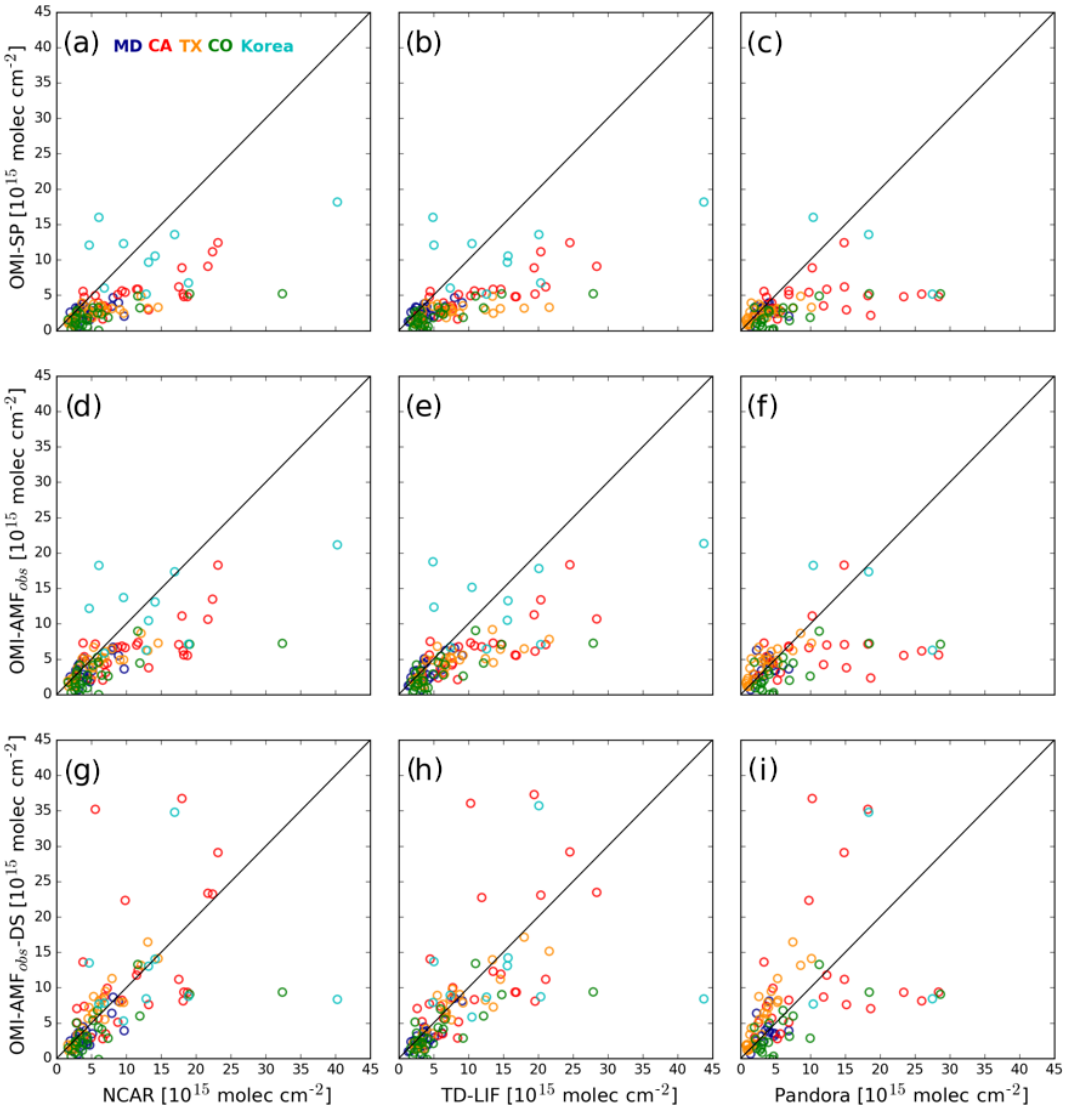

Figure 8. Comparison of tropospheric NO_2 columns from OMI with the data from NCAR **(a, d, g)**, TD-LIF **(b, e, h)**, and Pandora **(c, f, i)** instruments. OMI retrievals are performed using the default GMI **(a–c)** and observed NO_2 profiles **(d–i)**. In addition, OMI columns in **(g)–(i)** are downscaled with high-resolution (CMAQ and/or WRF-Chem) model simulations. Different colors represent the campaign locations.

ference in MD. OMI data are also lower than Pandora as shown in Fig. 8c. The magnitude of the difference and the degree of correlation with OMI vary for NCAR, TD-LIF, and Pandora measurements. This discrepancy between OMI, aircraft spiral columns, and Pandora local measurements is due to a combination of strong NO_2 spatial variation, the size of OMI pixels, and the placement of the sites, but OMI retrieval errors arising from inaccurate information in the AMF calculation, such as a priori NO_2 profiles, and potential errors in the validation sources themselves also contribute.

Figure 8d–f and Table A3 show the comparison after partially accounting for OMI retrieval errors arising from a priori NO_2 profiles taken from the GMI model. Replacing the model profiles with the NCAR and TD-LIF observed NO_2 profiles in the AMF calculations addresses the issues related to model inaccuracies, although the measured profiles may not necessarily represent the true average NO_2 over the entire OMI pixel (e.g., Fig. 4). Nevertheless, using observed profiles reduces OMI's mean differences with NCAR by 8 %–29.2 %, TD-LIF by 8.7 %–24.4 %, and Pandora by 6.8 %–24.2 %. Changes are largest in TX and smallest in CA and Korea. Correlations are either improved or remain similar.

Figure 8g–i and Table A4 show the comparison of OMI NO_2 columns derived using observed profiles with NCAR, TD-LIF, and Pandora observations after accounting for spatial variation in the NO_2 field as suggested by the CMAQ simulation. After downscaling, the agreement of OMI NO_2 columns improves further with NCAR by 1.1 %–41.5 %, TD-

LIF by 1.2 %–39.7 %, and Pandora by 1.2 %–33.2 %. The exceptions are MD for both aircraft and Pandora data and TX for Pandora data only. Changes are small in MD and Korea and large in CA and TX. The larger difference in TX is due to significant underestimation of NO_2 by Pandora instruments. The correlation improves in MD and TX but is reduced in CA, CO, and Korea. These results suggest that downscaling helps explain some of the discrepancies between OMI, aircraft, and Pandora observations. Variations among campaign locations may also point to difficulty related to the fidelity of the CMAQ simulations.

Figure 9 summarizes the comparison of OMI with aircraft and Pandora measurements. Here we present site mean columns observed from all measurements during the entire campaign periods. OMI captures the overall spatial variation in site means. In relatively cleaner places (NO_2 VCD $\leq 5 \times 10^{15}$ molec cm^{-2}), OMI agrees well with NCAR and TD-LIF columns. OMI values are generally lower in polluted areas.

3.4 Implications for satellite NO_2 validations

NO_2 measurements from a variety of instruments and techniques taken during the DISCOVER-AQ and KORUS-AQ field deployments provided a unique opportunity to assess correlative data and realize the strengths and limitations of the various measurements. Some of the techniques are still in a state of development and evaluation, and the data have not been fully validated. Additional complications arise when comparing measurements covering different areal extents. This is particularly true for a short-lived trace gas like NO_2 that has a large spatial gradient, especially in the boundary layer.

The NCAR and TD-LIF instruments onboard the same aircraft (P-3B during DISCOVER-AQ and DC-8 during KORUS-AQ) offer valuable insights on the vertical distribution of NO_2, a critical piece of information needed for satellite retrievals. Despite their adjacent locations on the aircraft, they did not sample the same air mass throughout each profile due to their different NO_2 measurement frequencies. Despite this, and even using independent measurement techniques with unique sources of uncertainties, NO_2 measurements from the two instruments exhibit excellent correlation and very good agreement in most cases. However, varying discrepancies between the two instruments among campaigns with campaign-average differences reaching up to 31.9 % are unlikely to be related solely to the sampling issues; they are rather related to issues pertaining to measurement methods. It is crucial to reconcile these differences and improve the accuracy of these measurements for the meaningful validation and improved error characterization of satellite NO_2 retrievals.

In situ aircraft spirals miss significant portions of the tropospheric NO_2 column, especially from the ground to the lowest level of the aircraft altitude, typically 200–300 m above ground level. In this analysis, we account for the missing portion above the aircraft profile by using coincidently sampled simulated NO_2 profiles. For the portion below the aircraft profile we extrapolate to surface monitor data. The latter step can be a significant error source, given that it assumes spatial homogeneity over the spiral domain. Additional errors could come from the use of different types of monitors that were deployed during the DISCOVER-AQ and KORUS-AQ campaigns (see Sect. 2.1.2). In particular, NO_2 data from molybdenum converter analyzers are biased high by variable amounts that are difficult to quantify and correct (e.g., Lamsal et al., 2008). The use of more accurate NO_2 monitors, such as photolytic converter analyzers, together with balloon-borne NO_2 sondes (Sluis et al., 2010) of similar accuracy would complement in situ aircraft profiles.

While total column NO_2 retrievals from the ground-based remote sensing Pandora instrument are useful to track temporal changes, their use for satellite validation or for comparing with aircraft spiral data can be onerous, particularly over locations with large NO_2 spatial gradients, such as cities. Pandora's field of view is so narrow that it serves as a point measurement. Additionally, Pandora data are subject to retrieval errors arising predominantly from the use of an incorrect reference spectrum as well as fixed temperature for the NO_2 cross section in the spectral fitting procedure. Failure to apply a reference spectrum derived using weeks of measurements from the same site often yields systematic biases in the retrieved NO_2 columns. Improved calibration and data processing are therefore needed to improve the Pandora data quality. Concurrent spatial NO_2 observations from other ground-based (e.g., multi-axis differential optical absorption spectroscopy – MAX-DOAS; Vlemmix et al., 2010) or airborne (e.g., Geostationary Trace gas and Aerosol Sensor Optimization – GeoTASO; Nowlan et al., 2016; Judd et al., 2019) platforms would facilitate intercomparison among measurements of different spatial scales.

The validation of NO_2 observations from any satellite instrument, including OMI, is complicated by a variety of factors, principally the ground area covered by the instrument's field of view. As discussed in Sect. 3.3, disagreement between partially (spatially and temporally) matched OMI NO_2 and validation measurements made near sources may be reasonably anticipated and ought to be expected. Therefore, it may be necessary to use a proper validation strategy, such as downscaling of satellite data using either observed or modeled NO_2 as presented in Fig. 8g–i and Table A4. It also underscores the need for comprehensive high-quality long-term observations for validation. Enhanced agreement with OMI retrievals revised using observed NO_2 profiles is indicative of retrieval errors from model-based a priori vertical NO_2 profile shapes (Fig. 8d–f, Table A3) and highlights the need for approaches to address the issue. Moreover, improved accuracy in other retrieval parameters, both surface and atmospheric, helps enhance the quality of satellite NO_2 retrievals (Laughner et al., 2019; Vasilkov et al., 2017, 2018; Lorente

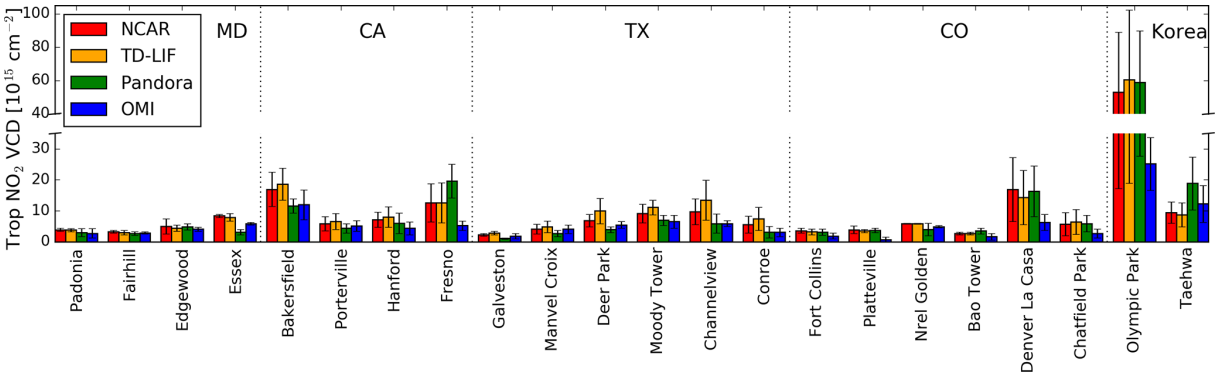

Figure 9. Site mean tropospheric NO_2 VCDs calculated from NCAR (blue), TD-LIF (orange), Pandora (green), and OMI (blue). The OMI data are derived using observed NO_2 profiles and downscaled using high-resolution model simulations. The vertical bars represent the standard deviations.

et al., 2018; Lin et al., 2014, 2015; Liu et al., 2019; Noguchi et al., 2014; Zhou et al., 2011)

4 Conclusions

We conducted a comprehensive intercomparison among various NO_2 measurements made during the five field deployments of DISCOVER-AQ and KORUS-AQ. The field campaigns were conducted in four US states (Maryland, California, Texas, and Colorado) and South Korea. The analyzed datasets were obtained from surface monitors, the NCAR and TD-LIF airborne instruments, ground-based Pandora instruments, and the space-based OMI. We investigated the data from 23 sites among the five campaigns when measurements from all these instruments were available. We focused on an analysis of tropospheric NO_2 column amounts. NO_2 mixing ratio measurements from the surface monitors and airborne instruments were merged and integrated to yield tropospheric columns, while the Pandora tropospheric columns were obtained by subtracting the OMI stratospheric column from Pandora total column observations.

In order to compare OMI NO_2 tropospheric columns with the available validation measurements, we used a combination of observed and simulated NO_2 vertical profiles to recalculate tropospheric NO_2 columns using the OMI Standard Product (OMNO2) version 3.1. To overcome the challenge of comparing OMI NO_2 with its relatively large pixel size to the airborne and ground-based measurements with small spatial scales, we additionally applied a downscaling technique, whereby OMI tropospheric NO_2 columns for each ground pixel are downscaled using high-resolution CMAQ (DISCOVER-AQ) or WRF-Chem (KORUS-AQ) model simulations. Therefore, the comparisons here include three kinds of OMI NO_2 tropospheric columns: (1) OMI Standard Product, (2) OMI data recalculated using observed NO_2 profiles, and (3) downscaled OMI NO_2 data.

The tropospheric columns from the NCAR and TD-LIF airborne instruments generally show good agreement, with a mean difference of 8.4 % and correlation coefficients in the 0.87–0.99 range. The Pandora columns also agree variably with the two airborne instruments, with the campaign-average difference in the range of 3 % to 54 %, but the correlation is not as good ($r = 0.18$–0.95) as between the two airborne instruments themselves. There are differences among the campaigns. In particular, all three instruments show the largest discrepancies in the TX campaign; TD-LIF is higher than NCAR by ~ 31.9 %, and Pandora data are lower by ~ 39 % and ~ 54 % compared to NCAR and TD-LIF measurements, respectively.

All three OMI NO_2 columns (Standard Product, based on observed NO_2 profiles, and downscaled) exhibit good correlation with the airborne and ground-based measurements. In terms of quantitative agreement, the OMI SP column is smaller than airborne and ground-based measurements. Retrievals using observed NO_2 profiles bring the OMI column closer to validation measurements. Applying downscaling to OMI data provides further improvement in agreement but little or insignificant change in correlation, perhaps due to the use of model simulations for downscaling.

As discussed in Sect. 3.3, disagreement between the comparatively large OMI pixel and smaller-scale ground and aircraft measurements is to be expected due to the large spatial variability of NO_2. Techniques such as the downscaling method shown here can reduce this discrepancy. However, the robust evaluation of NO_2 tropospheric column retrievals is further confounded by the current lack of agreement among ground-based and in-situ measurements. Future validation strategies for satellite observations of tropospheric column NO_2 will need to address these differences.

Appendix A

Table A1. Model options for each simulation. Note that all model options listed are for the domain used for the analysis.

	MD	CA	TX	CO	Korea
Dates	5/24/2011–8/1/2011	1/10/2013–2/28/2013	8/18/2013–10/1/2013	7/9/2014–08/20/2014	5/1/2016–5/31/2016
WRF model options					
Version	3.3	3.8	3.6.1	3.8.1	3.6.1
Model top	100 hPa	50 hPa	50 hPa	50 hPa	50 hPa
Spatial resolution	4 km	4 km	4 km	4 km	4 km
Vertical levels	34	35	45	37	52
Radiation	LW: RRTM SW: Goddard	LW: RRTMG SW: RRTMG	LW: RRTM SW: Goddard	LW: RRTMG SW: RRTMG	LW: RRTM SW: Goddard
Land surface model	Noah Land Surface Model (Tewari et al., 2004)	Pleim–Xiu (Pleim and Xiu, 2003)	Pleim–Xiu (Pleim and Xiu, 2003)	Unified Noah Land Surface Model	Unified Noah Land Surface Model
Boundary layer	YSU (Hong et al., 2006)	ACM2 (Pleim, 2007)	ACM2 (Pleim, 2007)	YSU (Hong et al., 2006)	MJY scheme
Meteor. init. and bound. cond.	12 km NAM	12 km NAM	12 km NAM	NCAR ECMWF	0.25 degree GFS
CMAQ model options					WRF-Chem
Version	5.0	5.2	5.0.2	5.2 beta	3.6.1 (modified)
Coupled?	No	Yes	No	No	Yes
Chemical mechanism	Carbon Bond (CB05) (Yarwood et al., 2005)	Carbon Bond (CB06, e51)	Carbon Bond (CB05) (Yarwood et al., 2005)	Carbon Bond (CB06, r3)	Reduced hydrocarbon (Pfister et al., 2014)
Aerosol	AE5	AERO6	AE5	AERO6	MOSAIC 4 bin
Chem. init. and bound. cond.	12 km CMAQ v5.0 simulation	12 km CMAQ v5.2 simulation	MOZART (outer domain)	RAQMS (outer domain)	24 km MACC for chemistry
Emissions	Described in Loughner et al. (2014)	4 km 2013 emissions, emissions based on the 2011 NEI with year-specific updates to EGU point sources (CEMs data), fires and mobile (MOBILE6)	2012 TCEQ anthropogenic emissions Biogenic Emission Inventory System (BEIS) calculated within CMAQ	Described in report	Described in Goldberg et al. (2019)[1] and Saide et al. (2019)

LW: longwave, SW: shortwave, RRTM: Rapid Radiative Transfer Model, RRTMG: Rapid Radiative Transfer Model for General Circulation Models, AE5: aerosols with aqueous extensions version 5, MOZART: Model for OZone and Related chemical Tracers, RAQMS: Real Time Air Quality Monitoring System, MACC: Monitoring Atmospheric Composition and Climate.

[1] https://www.colorado.gov/airquality/tech_doc_repository.aspx?action=open&file=FRAPPE-NCAR_Final_Report_July2017.pdf (last access: 5 September 2019).

Table A2. Summary of NO_2 comparison between the OMI Standard Product (OMI_{SP}) and NCAR, TD-LIF, and Pandora observations. The mean difference is calculated as OMI minus observations.

Campaign	NCAR vs. OMI_{SP}		TD-LIF vs. OMI_{SP}		Pandora vs. OMI_{SP}	
No. profs (Pandora)	Mean diff. (%)	r	Mean diff. (%)	r	Mean diff. (%)	r
MD 21 (14)	−40.7	0.39	−34.4	0.54	−21.8	0.21
CA 25 (22)	−53.8	0.77	−56.9	0.81	−58.5	0.24
TX 28 (26)	−54.9	0.65	−65.8	0.56	−26.9	0.65
CO 26 (21)	−67.5	0.73	−65.2	0.75	−68.2	0.72
Korea 11 (5)	−41.9	0.87	−47.9	0.87	−60.1	0.8
All 111 (88)	−51.9	0.82	−55.6	0.83	−54.6	0.84

Table A3. Same as A2, but for OMI using AMF_{obs} (OMI_{obs}).

Campaign	NCAR vs. OMI_{obs}		TD-LIF vs. OMI_{obs}		Pandora vs. OMI_{obs}	
No. profs (Pandora)	Mean diff. (%)	r	Mean diff. (%)	r	Mean diff. (%)	r
MD 21 (14)	−23.7	0.61	−17.6	0.7	2.4	0.3
CA 25 (22)	−42.4	0.73	−45.8	0.75	−47.9	0.2
TX 28 (26)	−25.5	0.82	−41.3	0.76	21.6	0.81
CO 26 (21)	−54.2	0.7	−50.5	0.71	−55.2	0.69
Korea 11 (5)	−33.9	0.87	−39.2	0.86	−53.3	0.79
All 111 (88)	−37.5	0.82	−41.5	0.82	−39.2	0.84

Table A4. Same as A2, but for OMI_{obs} with downscaling (OMI_{DS}).

Campaign	NCAR vs. OMI_{DS}		TD-LIF vs. OMI_{DS}		Pandora vs. OMI_{DS}	
No. profs (Pandora)	Mean diff. (%)	r	Mean diff. (%)	r	Mean diff. (%)	r
MD 21 (14)	−24.1	0.75	−18.0	0.85	0.8	0.31
CA 25 (22)	14.2	0.47	7.6	0.56	4.6	0.22
TX 28 (26)	9.5	0.94	−13.8	0.91	78.3	0.93
CO 26 (21)	−42.4	0.7	−37.7	0.71	−42.4	0.67
Korea 11 (5)	−32.8	0.73	−38.4	0.73	−52.1	0.48
All 111 (88)	−12.5	0.65	−18.0	0.68	−12.3	0.57

Data availability. Airborne, ground-based, and Pandora NO_2 data gathered during the DISCOVER-AQ and KORUS-AQ campaigns are available at the NASA Langley campaign data web archive (https://doi.org/10.5067/AIRCRAFT/DISCOVER-AQ/AEROSOL-TRACEGAS, DISCOVER-AQ Science Team, 2014; https://doi.org/10.5067/Suborbital/KORUSAQ/DATA01, KORUS-AQ Science Team, 2018). OMI NO_2 Standard Product (SP) data are available at the NASA Goddard Earth Sciences Data and Information Services Center (GES DISC) (https://doi.org/10.5067/Aura/OMI/DATA2017, Krotkov et al., 2019).

Author contributions. SC, LL, JJ, NAK, MFC, WHS, and KEP designed the data analysis. CPL, WA, GP, and PES provided the model simulations. RCC and AJW provided the airborne in situ measurements. JRH provided the ground-based Pandora measurements. SC, LL, MFC, WHS, CPL, WA, and PES wrote the paper with comments from all coauthors.

Competing interests. The authors declare that they have no conflict of interest.

Acknowledgements. The work was supported by NASA's Earth Science Division through Aura Science team and Atmospheric Composition Modeling and Analysis Program (ACMAP) grants. The Dutch–Finnish-built OMI is part of the NASA EOS Aura satellite payload. The OMI is managed by KNMI and the Netherlands Agency for Aerospace Programs (NIVR). NCAR is sponsored by the National Science Foundation (NSF). Pablo E. Saide would like to acknowledge support from NASA grant NNX11AI52G. The authors thank all principal investigators and their staff for providing ground- and aircraft-based NO_2 measurements during the DISCOVER-AQ and KORUS-AQ campaigns.

Financial support. This research has been supported by the National Aeronautics and Space Administration, Goddard Space Flight Center (grant no. 80NSSC17K0676).

Review statement. This paper was edited by Michel Van Roozendael and reviewed by three anonymous referees.

References

Anderson, D. C., Loughner, C. P., Diskin, G., Weinheimer, A., Canty, T. P., Salawitch, R. J., Worden, H. M., Fried, A., Mikoviny, T., Wisthaler, A., and Dickerson, R. R.: Measured and modeled CO and NOy in DISCOVER-AQ: An evaluation of emissions and chemistry over the eastern US, Atmos. Environ., 96, 78–87, https://doi.org/10.1016/j.atmosenv.2014.07.004, 2014.

Bechle, M. J., Millet, D. B., and Marshall, J. D.: Remote sensing of exposure to NO_2: Satellite versus ground-based measurement in a large urban area, Atmos. Environ., 69, 345–353, https://doi.org/10.1016/j.atmosenv.2012.11.046, 2013.

Beirle, S., Platt, U., Wenig, M., and Wagner, T.: Weekly cycle of NO_2 by GOME measurements: a signature of anthropogenic sources, Atmos. Chem. Phys., 3, 2225–2232, https://doi.org/10.5194/acp-3-2225-2003, 2003.

Beirle, S., Boersma, K. F., Platt, U., Lawrence, M. G., and Wagner, T.: Megacity emissions and lifetimes of nitrogen oxides probed from space, Science, 333, 1737–1739, https://doi.org/10.1126/science.1207824, 2011.

Boersma, K. F., Jacob, D. J., Bucsela, E. J., Perring, A. E., Dirksen, R., van der A, R. J., Yantosca, R. M., Park, R. J., Wenig, M. O., Bertram, T. H., and Cohen, R. C.: Validation of OMI tropospheric NO_2 Observations During INTEX-B and application to constrain NO_x emissions over the eastern United States and Mexico, Atmos. Environ., 42, 4480–4497, https://doi.org/10.1016/j.atmosenv.2008.02.004, 2008.

Brion, J., Chakir, A., Daumont, D., Malicet, J., and Parisse, C.: High-resolution laboratory absorption cross section of O_3. Temperature effect, Chem. Phys. Lett., 213, 610–612, https://doi.org/10.1016/0009-2614(93)89169-I, 1993.

Bucsela, E. J., Celarier, E. A., Wenig, M. O., Gleason, J. F., Veefkind, J. P., Boersma, K. F., and Brinksma, E. J.: Algorithm for NO_2 vertical column retrieval from the ozone monitoring instrument, IEEE T. Geosci. Remote, 44, 1245–1258, https://doi.org/10.1109/TGRS.2005.863715, 2006.

Bucsela, E. J., Perring, A. E., Cohen, R. C., Boersma, K. F., Celarier, E. A., Gleason, J. F., Wenig, M. O., Bertram, T. H., Wooldridge, P. J., Dirksen, R., and Veefkind, J. P.: Comparison of tropospheric NO_2 from in situ aircraft measurements with near-real-time and standard product data from OMI, J. Geophys. Res.-Atmos., 113, D16S31, https://doi.org/10.1029/2007JD008838, 2008.

Bucsela, E. J., Pickering, K. E., Huntemann, T. L., Cohen, R. C., Perring, A., Gleason, J. F., Blakeslee, R. J., Albrecht, R. I., Holzworth, R., Cipriani, J. P., Vargas-Navarro, D., Mora-Segura, I., Pacheco-Hernández, A., and Laporte-Molina, S.: Lightning-generated NO_x seen by the Ozone Monitoring Instrument during NASA's Tropical Composition, Cloud and Climate Coupling Experiment (TC4), J. Geophys. Res.-Atmos., 115, D00J10, https://doi.org/10.1029/2009JD013118, 2010.

Bucsela, E. J., Krotkov, N. A., Celarier, E. A., Lamsal, L. N., Swartz, W. H., Bhartia, P. K., Boersma, K. F., Veefkind, J. P., Gleason, J. F., and Pickering, K. E.: A new stratospheric and tropospheric NO_2 retrieval algorithm for nadir-viewing satellite instruments: applications to OMI, Atmos. Meas. Tech., 6, 2607–2626, https://doi.org/10.5194/amt-6-2607-2013, 2013.

Burkholder, J., Sander, S., Abbatt, J., Barker, J., Huie, R., Kolb, C., Kurylo, M., Orkin, V., Wilmouth, D., and Wine, P.: Chemical Kinetics and Photochemical Data for Use in Atmospheric Studies: Evaluation Number 18, Tech. rep., JPL Publication 15-10, Pasadena, California, USA, 2015.

Byun, D. and Schere, K.: Review of the Governing Equations, Computational Algorithms and Other Components of the Models-3 Community Multiscale Air Quality (CMAQ) Modeling System, Appl. Mech. Rev., 59, 51–78, 2005.

Celarier, E. A., Brinksma, E. J., Gleason, J. F., Veefkind, J. P., Cede, A., Herman, J. R., Ionov, D., Goutail, F., Pommereau, J.-P., Lambert, J.-C., Roozendael, M. v., Pinardi, G., Wittrock, F., Schönhardt, A., Richter, A., Ibrahim, O. W., Wagner, T., Bojkov, B.,

Mount, G., Spinei, E., Chen, C. M., Pongetti, T. J., Sander, S. P., Bucsela, E. J., Wenig, M. O., Swart, D. P. J., Volten, H., Kroon, M., and Levelt, P. F.: Validation of Ozone Monitoring Instrument nitrogen dioxide columns, J. Geophys. Res.-Atmos., 113, D15S15, https://doi.org/10.1029/2007JD008908, 2008.

Chin, M., Diehl, T., Tan, Q., Prospero, J. M., Kahn, R. A., Remer, L. A., Yu, H., Sayer, A. M., Bian, H., Geogdzhayev, I. V., Holben, B. N., Howell, S. G., Huebert, B. J., Hsu, N. C., Kim, D., Kucsera, T. L., Levy, R. C., Mishchenko, M. I., Pan, X., Quinn, P. K., Schuster, G. L., Streets, D. G., Strode, S. A., Torres, O., and Zhao, X.-P.: Multi-decadal aerosol variations from 1980 to 2009: a perspective from observations and a global model, Atmos. Chem. Phys., 14, 3657–3690, https://doi.org/10.5194/acp-14-3657-2014, 2014.

Cooper, M., Martin, R. V., Padmanabhan, A., and Henze, D. K.: Comparing mass balance and adjoint methods for inverse modeling of nitrogen dioxide columns for global nitrogen oxide emissions, J. Geophys. Res.-Atmos., 122, 4718–4734, https://doi.org/10.1002/2016JD025985, 2017.

Dave, J. V.: Importance of higher order scattering in a molecular atmosphere, J. Opt. Soc. Am., 54, 307–315, https://doi.org/10.1364/JOSA.54.000307, 1964.

DeLand, M. and Marchenko, S.: The solar chromospheric Ca and Mg indices from Aura OMI, J. Geophys. Res.-Atmos., 118, 3415–3423, https://doi.org/10.1002/jgrd.50310, 2013.

de Wildt, M. D. R., Eskes, H., and Boersma, K. F.: The global economic cycle and satellite-derived NO_2 trends over shipping lanes, Geophys. Res. Lett., 39, L01802, https://doi.org/10.1029/2011GL049541, 2012.

Dickerson, R. R., Anderson, D. C., and Ren, X.: On the use of data from commercial NO_x analyzers for air pollution studies, Atmos. Environ., 214, 116873, https://doi.org/10.1016/j.atmosenv.2019.116873, 2019.

DISCOVER-AQ Science Team: DISCOVER-AQ P-3B aircraft in-situ trace gas measurements version 1 – ICARTT File, NASA Langley Atmospheric Science Data Center DAAC, https://doi.org/10.5067/AIRCRAFT/DISCOVER-AQ/AEROSOL-TRACEGAS, 2014.

Dobber, M., Kleipool, Q., Dirksen, R., Levelt, P., Jaross, G., Taylor, S., Kelly, T., Flynn, L., Leppelmeier, G., and Rozemeijer, N.: Validation of Ozone Monitoring Instrument level 1b data products, J. Geophys. Res.-Atmos., 113, D15S06, https://doi.org/10.1029/2007JD008665, 2008.

Duncan, B. N., Strahan, S. E., Yoshida, Y., Steenrod, S. D., and Livesey, N.: Model study of the cross-tropopause transport of biomass burning pollution, Atmos. Chem. Phys., 7, 3713–3736, https://doi.org/10.5194/acp-7-3713-2007, 2007.

Duncan, B. N., Yoshida, Y., de Foy, B., Lamsal, L. N., Streets, D. G., Lu, Z., Pickering, K. E., and Krotkov, N. A.: The observed response of Ozone Monitoring Instrument (OMI) NO_2 columns to NO_x emission controls on power plants in the United States: 2005–2011, Atmos. Environ., 81, 102–111, https://doi.org/10.1016/j.atmosenv.2013.08.068, 2013.

Dunlea, E. J., Herndon, S. C., Nelson, D. D., Volkamer, R. M., San Martini, F., Sheehy, P. M., Zahniser, M. S., Shorter, J. H., Wormhoudt, J. C., Lamb, B. K., Allwine, E. J., Gaffney, J. S., Marley, N. A., Grutter, M., Marquez, C., Blanco, S., Cardenas, B., Retama, A., Ramos Villegas, C. R., Kolb, C. E., Molina, L. T., and Molina, M. J.: Evaluation of nitrogen dioxide chemiluminescence monitors in a polluted urban environment, Atmos. Chem. Phys., 7, 2691–2704, https://doi.org/10.5194/acp-7-2691-2007, 2007.

Fehsenfeld, F. C., Drummond, J. W., Roychowdhury, U. K., Galvin, P. J., Williams, E. J., Buhr, M. P., Parrish, D. D., Hübler, G., Langford, A. O., Calvert, J. G., Ridley, B. A., Grahek, F., Heikes, B. G., Kok, G. L., Shetter, J. D., Walega, J. G., Elsworth, C. M., Norton, R. B., Fahey, D. W., Murphy, P. C., Hovermale, C., Mohnen, V. A., Demerjian, K. L., Mackay, G. I., and Schiff, H. I.: Intercomparison of NO_2 measurement techniques, J. Geophys. Res.-Atmos., 95, 3579–3597, https://doi.org/10.1029/JD095iD04p03579, 1990.

Geddes, J. A. and Martin, R. V.: Global deposition of total reactive nitrogen oxides from 1996 to 2014 constrained with satellite observations of NO_2 columns, Atmos. Chem. Phys., 17, 10071–10091, https://doi.org/10.5194/acp-17-10071-2017, 2017.

Gelaro, R., McCarty, W., Suárez, M. J., Todling, R., Molod, A., Takacs, L., Randles, C. A., Darmenov, A., Bosilovich, M. G., Reichle, R., Wargan, K., Coy, L., Cullather, R., Draper, C., Akella, S., Buchard, V., Conaty, A., da Silva, A. M., Gu, W., Kim, G.-K., Koster, R., Lucchesi, R., Merkova, D., Nielsen, J. E., Partyka, G., Pawson, S., Putman, W., Rienecker, M., Schubert, S. D., Sienkiewicz, M., and Zhao, B.: The Modern-Era Retrospective Analysis for Research and Applications, Version 2 (MERRA-2), J. Climate, 30, 5419–5454, https://doi.org/10.1175/JCLI-D-16-0758.1, 2017.

Ghude, S. D., Lal, D. M., Beig, G., van der A, R., and Sable, D.: Rain-Induced Soil NO_x Emission From India During the Onset of the Summer Monsoon: A Satellite Perspective, J. Geophys. Res.-Atmos., 115, D16304, https://doi.org/10.1029/2009JD013367, 2010.

Ghude, S. D., Kulkarni, S. H., Jena, C., Pfister, G. G., Beig, G., Fadnavis, S., and van der A, R. J.: Application of satellite observations for identifying regions of dominant sources of nitrogen oxides over the Indian Subcontinent, J. Geophys. Res.-Atmos., 118, 1075–1089, https://doi.org/10.1029/2012JD017811, 2013a.

Ghude, S. D., Pfister, G. G., Jena, C., A, R. J. v. d., Emmons, L. K., and Kumar, R.: Satellite constraints of nitrogen oxide (NO_x) emissions from India based on OMI observations and WRF-Chem simulations, Geophys. Res. Lett., 40, 423–428, https://doi.org/10.1002/grl.50065, 2013b.

Goldberg, D. L., Lamsal, L. N., Loughner, C. P., Swartz, W. H., Lu, Z., and Streets, D. G.: A high-resolution and observationally constrained OMI NO_2 satellite retrieval, Atmos. Chem. Phys., 17, 11403–11421, https://doi.org/10.5194/acp-17-11403-2017, 2017.

Goldberg, D. L., Saide, P. E., Lamsal, L. N., de Foy, B., Lu, Z., Woo, J.-H., Kim, Y., Kim, J., Gao, M., Carmichael, G., and Streets, D. G.: A top-down assessment using OMI NO_2 suggests an underestimate in the NO_x emissions inventory in Seoul, South Korea, during KORUS-AQ, Atmos. Chem. Phys., 19, 1801–1818, https://doi.org/10.5194/acp-19-1801-2019, 2019.

Grell, G. A., Peckham, S. E., Schmitz, R., McKeen, S. A., Frost, G., Skamarock, W. C., and Eder, B.: Fully coupled "online" chemistry within the WRF model, Atmos. Environ., 39, 6957–6975, https://doi.org/10.1016/j.atmosenv.2005.04.027, 2005.

Hains, J. C., Boersma, K. F., Kroon, M., Dirksen, R. J., Cohen, R. C., Perring, A. E., Bucsela, E., Volten, H., Swart, D. P. J., Richter, A., Wittrock, F., Schoenhardt, A., Wagner, T., Ibrahim,

O. W., Roozendael, M. v., Pinardi, G., Gleason, J. F., Veefkind, J. P., and Levelt, P.: Testing and improving OMI DOMINO tropospheric NO_2 using observations from the DANDELIONS and INTEX-B validation campaigns, J. Geophys. Res.-Atmos., 115, D05301, https://doi.org/10.1029/2009JD012399, 2010.

Herman, J., Cede, A., Spinei, E., Mount, G., Tzortziou, M., and Abuhassan, N.: NO_2 column amounts from ground-based Pandora and MFDOAS spectrometers using the direct-sun DOAS technique: Intercomparisons and application to OMI validation, J. Geophys. Res.-Atmos., 114, D13307, https://doi.org/10.1029/2009JD011848, 2009.

Herman, J., Spinei, E., Fried, A., Kim, J., Kim, J., Kim, W., Cede, A., Abuhassan, N., and Segal-Rozenhaimer, M.: NO_2 and HCHO measurements in Korea from 2012 to 2016 from Pandora spectrometer instruments compared with OMI retrievals and with aircraft measurements during the KORUS-AQ campaign, Atmos. Meas. Tech., 11, 4583–4603, https://doi.org/10.5194/amt-11-4583-2018, 2018.

Herron-Thorpe, F. L., Lamb, B. K., Mount, G. H., and Vaughan, J. K.: Evaluation of a regional air quality forecast model for tropospheric NO_2 columns using the OMI/Aura satellite tropospheric NO_2 product, Atmos. Chem. Phys., 10, 8839–8854, https://doi.org/10.5194/acp-10-8839-2010, 2010.

Hilboll, A., Richter, A., and Burrows, J. P.: Long-term changes of tropospheric NO_2 over megacities derived from multiple satellite instruments, Atmos. Chem. Phys., 13, 4145–4169, https://doi.org/10.5194/acp-13-4145-2013, 2013.

Hong, S.-Y., Noh, Y., and Dudhia, J.: A new vertical diffusion package with an explicit treatment of entrainment processes, Mon. Weather Rev., 134, 2318–2341, https://doi.org/10.1175/MWR3199.1, 2006.

Huijnen, V., Eskes, H. J., Poupkou, A., Elbern, H., Boersma, K. F., Foret, G., Sofiev, M., Valdebenito, A., Flemming, J., Stein, O., Gross, A., Robertson, L., D'Isidoro, M., Kioutsioukis, I., Friese, E., Amstrup, B., Bergstrom, R., Strunk, A., Vira, J., Zyryanov, D., Maurizi, A., Melas, D., Peuch, V.-H., and Zerefos, C.: Comparison of OMI NO_2 tropospheric columns with an ensemble of global and European regional air quality models, Atmos. Chem. Phys., 10, 3273–3296, https://doi.org/10.5194/acp-10-3273-2010, 2010.

Ialongo, I., Herman, J., Krotkov, N., Lamsal, L., Boersma, K. F., Hovila, J., and Tamminen, J.: Comparison of OMI NO_2 observations and their seasonal and weekly cycles with ground-based measurements in Helsinki, Atmos. Meas. Tech., 9, 5203–5212, https://doi.org/10.5194/amt-9-5203-2016, 2016.

Irie, H., Boersma, K. F., Kanaya, Y., Takashima, H., Pan, X., and Wang, Z. F.: Quantitative bias estimates for tropospheric NO_2 columns retrieved from SCIAMACHY, OMI, and GOME-2 using a common standard for East Asia, Atmos. Meas. Tech., 5, 2403–2411, https://doi.org/10.5194/amt-5-2403-2012, 2012.

Jaeglé, L., Steinberger, L., Martin, R. V., and Chance, K.: Global partitioning of NO_x sources using satellite observations: Relative roles of fossil fuel combustion, biomass burning and soil emissions, Faraday Discuss., 130, 407–423, https://doi.org/10.1039/B502128F, 2005.

Judd, L. M., Al-Saadi, J. A., Janz, S. J., Kowalewski, M. G., Pierce, R. B., Szykman, J. J., Valin, L. C., Swap, R., Cede, A., Mueller, M., Tiefengraber, M., Abuhassan, N., and Williams, D.: Evaluating the impact of spatial resolution on tropospheric NO_2 column comparisons within urban areas using high-resolution airborne data, Atmos. Meas. Tech., 12, 6091–6111, https://doi.org/10.5194/amt-12-6091-2019, 2019.

Kebabian, P. L., Wood, E. C., Herndon, S. C., and Freedman, A.: A practical alternative to chemiluminescence-based detection of nitrogen dioxide: cavity attenuated phase shift spectroscopy, Environ. Sci. Technol., 42, 6040–6045, https://doi.org/10.1021/es703204j, 2008.

Kim, H. C., Lee, P., Judd, L., Pan, L., and Lefer, B.: OMI NO_2 column densities over North American urban cities: the effect of satellite footprint resolution, Geosci. Model Dev., 9, 1111–1123, https://doi.org/10.5194/gmd-9-1111-2016, 2016.

Kim, H. C., Lee, S.-M., Chai, T., Ngan, F., Pan, L., and Lee, P.: A conservative downscaling of satellite-detected chemical compositions: NO_2 column densities of OMI, GOME-2, and CMAQ, Remote Sensing, 10, 1001, https://doi.org/10.3390/rs10071001, 2018.

Kim, S.-W., Heckel, A., Frost, G. J., Richter, A., Gleason, J., Burrows, J. P., McKeen, S., Hsie, E.-Y., Granier, C., and Trainer, M.: NO_2 columns in the western United States observed from space and simulated by a regional chemistry model and their implications for NO_x emissions, J. Geophys. Res.-Atmos., 114, D11301, https://doi.org/10.1029/2008JD011343, 2009.

Konovalov, I. B., Beekmann, M., Richter, A., and Burrows, J. P.: Inverse modelling of the spatial distribution of NO_x emissions on a continental scale using satellite data, Atmos. Chem. Phys., 6, 1747–1770, https://doi.org/10.5194/acp-6-1747-2006, 2006.

KORUS-AQ Science Team: KORUS-AQ airborne mission in-situ trace gas measurements version 1 – ICARTT File, NASA Langley Atmospheric Science Data Center DAAC, https://doi.org/10.5067/Suborbital/KORUSAQ/DATA01, 2018.

Krotkov, N. A., McLinden, C. A., Li, C., Lamsal, L. N., Celarier, E. A., Marchenko, S. V., Swartz, W. H., Bucsela, E. J., Joiner, J., Duncan, B. N., Boersma, K. F., Veefkind, J. P., Levelt, P. F., Fioletov, V. E., Dickerson, R. R., He, H., Lu, Z., and Streets, D. G.: Aura OMI observations of regional SO_2 and NO_2 pollution changes from 2005 to 2015, Atmos. Chem. Phys., 16, 4605–4629, https://doi.org/10.5194/acp-16-4605-2016, 2016.

Krotkov, N. A., Lamsal, L. N., Celarier, E. A., Swartz, W. H., Marchenko, S. V., Bucsela, E. J., Chan, K. L., Wenig, M., and Zara, M.: The version 3 OMI NO_2 standard product, Atmos. Meas. Tech., 10, 3133–3149, https://doi.org/10.5194/amt-10-3133-2017, 2017.

Krotkov, N. A., Lamsal, L. N., Marchenko, S. V., Celarier, E. A., Bucsela, E. J., Swartz, W. H., Joiner, J., and the OMI core team: OMI/Aura nitrogen dioxide (NO_2) total and tropospheric column 1-orbit L2 swath 13x24 km V003, Greenbelt, MD, USA, Goddard Earth Sciences Data and Information Services Center (GES DISC), https://doi.org/10.5067/Aura/OMI/DATA2017, 2019 OMI/Aura Nitrogen Dioxide (NO_2) Total and Tropospheric Column 1-orbit L2 Swath 13x24 km V003, Greenbelt, MD, USA, Goddard Earth Sciences Data and Information Services Center (GES DISC), https://doi.org/10.5067/Aura/OMI/DATA2017, 2019.

Lamsal, L. N., Martin, R. V., Donkelaar, A. V., Steinbacher, M., Celarier, E. A., Bucsela, E., Dunlea, E. J., and Pinto, J. P.: Ground-level nitrogen dioxide concentrations inferred from the satellite-borne Ozone Monitoring Instrument, J. Geophys. Res.-

Atmos., 113, D16308, https://doi.org/10.1029/2007JD009235, 2008.

Lamsal, L. N., Martin, R. V., Donkelaar, A. v., Celarier, E. A., Bucsela, E. J., Boersma, K. F., Dirksen, R., Luo, C., and Wang, Y.: Indirect validation of tropospheric nitrogen dioxide retrieved from the OMI satellite instrument: Insight into the seasonal variation of nitrogen oxides at northern midlatitudes, J. Geophys. Res.-Atmos., 115, D05302, https://doi.org/10.1029/2009JD013351, 2010.

Lamsal, L. N., Martin, R. V., Padmanabhan, A., van Donkelaar, A., Zhang, Q., Sioris, C. E., Chance, K., Kurosu, T. P., and Newchurch, M. J.: Application of satellite observations for timely updates to global anthropogenic NO_x emission inventories, Geophys. Res. Lett., 38, L05810, https://doi.org/10.1029/2010GL046476, 2011.

Lamsal, L. N., Krotkov, N. A., Celarier, E. A., Swartz, W. H., Pickering, K. E., Bucsela, E. J., Gleason, J. F., Martin, R. V., Philip, S., Irie, H., Cede, A., Herman, J., Weinheimer, A., Szykman, J. J., and Knepp, T. N.: Evaluation of OMI operational standard NO_2 column retrievals using in situ and surface-based NO_2 observations, Atmos. Chem. Phys., 14, 11587–11609, https://doi.org/10.5194/acp-14-11587-2014, 2014.

Lamsal, L. N., Duncan, B. N., Yoshida, Y., Krotkov, N. A., Pickering, K. E., Streets, D. G., and Lu, Z.: U.S. NO_2 trends (2005–2013): EPA Air Quality System (AQS) data versus improved observations from the Ozone Monitoring Instrument (OMI), Atmos. Environ., 110, 130–143, https://doi.org/10.1016/j.atmosenv.2015.03.055, 2015.

Lamsal, L. N., Janz, S. J., Krotkov, N. A., Pickering, K. E., Spurr, R. J. D., Kowalewski, M. G., Loughner, C. P., Crawford, J. H., Swartz, W. H., and Herman, J. R.: High-resolution NO_2 observations from the Airborne Compact Atmospheric Mapper: retrieval and validation, J. Geophys. Res.-Atmos., 122, 1953–1970, https://doi.org/10.1002/2016JD025483, 2017.

Laughner, J. L., Zare, A., and Cohen, R. C.: Effects of daily meteorology on the interpretation of space-based remote sensing of NO_2, Atmos. Chem. Phys., 16, 15247–15264, https://doi.org/10.5194/acp-16-15247-2016, 2016.

Laughner, J. L., Zhu, Q., and Cohen, R. C.: Evaluation of version 3.0B of the BEHR OMI NO_2 product, Atmos. Meas. Tech., 12, 129–146, https://doi.org/10.5194/amt-12-129-2019, 2019.

Levelt, P. F., Oord, G. H. J. v. d., Dobber, M. R., Malkki, A., Huib Visser, Johan de Vries, Stammes, P., Lundell, J. O. V., and Saari, H.: The ozone monitoring instrument, IEEE T. Geosci. Remote, 44, 1093–1101, https://doi.org/10.1109/TGRS.2006.872333, 2006.

Levelt, P. F., Joiner, J., Tamminen, J., Veefkind, J. P., Bhartia, P. K., Stein Zweers, D. C., Duncan, B. N., Streets, D. G., Eskes, H., van der A, R., McLinden, C., Fioletov, V., Carn, S., de Laat, J., DeLand, M., Marchenko, S., McPeters, R., Ziemke, J., Fu, D., Liu, X., Pickering, K., Apituley, A., González Abad, G., Arola, A., Boersma, F., Chan Miller, C., Chance, K., de Graaf, M., Hakkarainen, J., Hassinen, S., Ialongo, I., Kleipool, Q., Krotkov, N., Li, C., Lamsal, L., Newman, P., Nowlan, C., Suleiman, R., Tilstra, L. G., Torres, O., Wang, H., and Wargan, K.: The Ozone Monitoring Instrument: overview of 14 years in space, Atmos. Chem. Phys., 18, 5699–5745, https://doi.org/10.5194/acp-18-5699-2018, 2018.

Lin, J.-T.: Satellite constraint for emissions of nitrogen oxides from anthropogenic, lightning and soil sources over East China on a high-resolution grid, Atmos. Chem. Phys., 12, 2881–2898, https://doi.org/10.5194/acp-12-2881-2012, 2012.

Lin, J.-T., McElroy, M. B., and Boersma, K. F.: Constraint of anthropogenic NO_x emissions in China from different sectors: a new methodology using multiple satellite retrievals, Atmos. Chem. Phys., 10, 63–78, https://doi.org/10.5194/acp-10-63-2010, 2010.

Lin, J.-T., Martin, R. V., Boersma, K. F., Sneep, M., Stammes, P., Spurr, R., Wang, P., Van Roozendael, M., Clémer, K., and Irie, H.: Retrieving tropospheric nitrogen dioxide from the Ozone Monitoring Instrument: effects of aerosols, surface reflectance anisotropy, and vertical profile of nitrogen dioxide, Atmos. Chem. Phys., 14, 1441–1461, https://doi.org/10.5194/acp-14-1441-2014, 2014.

Lin, J.-T., Liu, M.-Y., Xin, J.-Y., Boersma, K. F., Spurr, R., Martin, R., and Zhang, Q.: Influence of aerosols and surface reflectance on satellite NO_2 retrieval: seasonal and spatial characteristics and implications for NO_x emission constraints, Atmos. Chem. Phys., 15, 11217–11241, https://doi.org/10.5194/acp-15-11217-2015, 2015.

Liu, F., van der A, R. J., Eskes, H., Ding, J., and Mijling, B.: Evaluation of modeling NO_2 concentrations driven by satellite-derived and bottom-up emission inventories using in situ measurements over China, Atmos. Chem. Phys., 18, 4171–4186, https://doi.org/10.5194/acp-18-4171-2018, 2018.

Liu, M., Lin, J., Boersma, K. F., Pinardi, G., Wang, Y., Chimot, J., Wagner, T., Xie, P., Eskes, H., Van Roozendael, M., Hendrick, F., Wang, P., Wang, T., Yan, Y., Chen, L., and Ni, R.: Improved aerosol correction for OMI tropospheric NO_2 retrieval over East Asia: constraint from CALIOP aerosol vertical profile, Atmos. Meas. Tech., 12, 1–21, https://doi.org/10.5194/amt-12-1-2019, 2019.

Lorente, A., Boersma, K. F., Stammes, P., Tilstra, L. G., Richter, A., Yu, H., Kharbouche, S., and Muller, J.-P.: The importance of surface reflectance anisotropy for cloud and NO_2 retrievals from GOME-2 and OMI, Atmos. Meas. Tech., 11, 4509–4529, https://doi.org/10.5194/amt-11-4509-2018, 2018.

Loughner, C. P., Tzortziou, M., Follette-Cook, M., Pickering, K. E., Goldberg, D., Satam, C., Weinheimer, A., Crawford, J. H., Knapp, D. J., Montzka, D. D., Diskin, G. S., and Dickerson, R. R.: Impact of bay-breeze circulations on surface air quality and boundary layer export, J. Appl. Meteorol. Clim., 53, 1697–1713, https://doi.org/10.1175/JAMC-D-13-0323.1, 2014.

Lu, Z. and Streets, D. G.: Increase in NO_x emissions from Indian thermal power plants during 1996–2010: unit-based inventories and multisatellite observations, Environ. Sci. Technol., 46, 7463–7470, https://doi.org/10.1021/es300831w, 2012.

Marchenko, S., Krotkov, N. A., Lamsal, L. N., Celarier, E. A., Swartz, W. H., and Bucsela, E. J.: Revising the slant column density retrieval of nitrogen dioxide observed by the Ozone Monitoring Instrument, J. Geophys. Res.-Atmos., 120, 5670–5692, https://doi.org/10.1002/2014JD022913, 2015.

Martin, R. V., Chance, K., Jacob, D. J., Kurosu, T. P., Spurr, R. J. D., Bucsela, E., Gleason, J. F., Palmer, P. I., Bey, I., Fiore, A. M., Li, Q., Yantosca, R. M., and Koelemeijer, R. B. A.: An improved retrieval of tropospheric nitrogen dioxide from

GOME, J. Geophys. Res.-Atmos., 107, ACH 9-1–ACH 9-21, https://doi.org/10.1029/2001JD001027, 2002.

Martin, R. V., Jacob, D. J., Chance, K., Kurosu, T. P., Palmer, P. I., and Evans, M. J.: Global inventory of nitrogen oxide emissions constrained by space-based observations of NO_2 columns, J. Geophys. Res.-Atmos., 108, 4537, https://doi.org/10.1029/2003JD003453, 2003.

McLinden, C. A., Fioletov, V., Boersma, K. F., Kharol, S. K., Krotkov, N., Lamsal, L., Makar, P. A., Martin, R. V., Veefkind, J. P., and Yang, K.: Improved satellite retrievals of NO_2 and SO_2 over the Canadian oil sands and comparisons with surface measurements, Atmos. Chem. Phys., 14, 3637–3656, https://doi.org/10.5194/acp-14-3637-2014, 2014.

Mebust, A. K. and Cohen, R. C.: Observations of a seasonal cycle in NO_x emissions from fires in African woody savannas, Geophys. Res. Lett., 40, 1451–1455, https://doi.org/10.1002/grl.50343, 2013.

Miyazaki, K., Eskes, H., Sudo, K., Boersma, K. F., Bowman, K., and Kanaya, Y.: Decadal changes in global surface NO_x emissions from multi-constituent satellite data assimilation, Atmos. Chem. Phys., 17, 807–837, https://doi.org/10.5194/acp-17-807-2017, 2017.

Murray, L. T., Jacob, D. J., Logan, J. A., Hudman, R. C., and Koshak, W. J.: Optimized regional and interannual variability of lightning in a global chemical transport model constrained by LIS/OTD satellite data, J. Geophys. Res.-Atmos., 117, D20307, https://doi.org/10.1029/2012JD017934, 2012.

Murray, L. T., Mickley, L. J., Kaplan, J. O., Sofen, E. D., Pfeiffer, M., and Alexander, B.: Factors controlling variability in the oxidative capacity of the troposphere since the Last Glacial Maximum, Atmos. Chem. Phys., 14, 3589–3622, https://doi.org/10.5194/acp-14-3589-2014, 2014.

Noguchi, K., Richter, A., Rozanov, V., Rozanov, A., Burrows, J. P., Irie, H., and Kita, K.: Effect of surface BRDF of various land cover types on geostationary observations of tropospheric NO_2, Atmos. Meas. Tech., 7, 3497–3508, https://doi.org/10.5194/amt-7-3497-2014, 2014.

Novotny, E. V., Bechle, M. J., Millet, D. B., and Marshall, J. D.: National satellite-based land-use regression: NO_2 in the United States, Environ. Sci. Technol., 45, 4407–4414, https://doi.org/10.1021/es103578x, 2011.

Nowlan, C. R., Martin, R. V., Philip, S., Lamsal, L. N., Krotkov, N. A., Marais, E. A., Wang, S., and Zhang, Q.: Global dry deposition of nitrogen dioxide and sulfur dioxide inferred from space-based measurements, Global Biogeochem. Cy., 28, 1025–1043, https://doi.org/10.1002/2014GB004805, 2014.

Nowlan, C. R., Liu, X., Leitch, J. W., Chance, K., González Abad, G., Liu, C., Zoogman, P., Cole, J., Delker, T., Good, W., Murcray, F., Ruppert, L., Soo, D., Follette-Cook, M. B., Janz, S. J., Kowalewski, M. G., Loughner, C. P., Pickering, K. E., Herman, J. R., Beaver, M. R., Long, R. W., Szykman, J. J., Judd, L. M., Kelley, P., Luke, W. T., Ren, X., and Al-Saadi, J. A.: Nitrogen dioxide observations from the Geostationary Trace gas and Aerosol Sensor Optimization (GeoTASO) airborne instrument: Retrieval algorithm and measurements during DISCOVER-AQ Texas 2013, Atmos. Meas. Tech., 9, 2647–2668, https://doi.org/10.5194/amt-9-2647-2016, 2016.

Nowlan, C. R., Liu, X., Janz, S. J., Kowalewski, M. G., Chance, K., Follette-Cook, M. B., Fried, A., González Abad, G., Herman, J. R., Judd, L. M., Kwon, H.-A., Loughner, C. P., Pickering, K. E., Richter, D., Spinei, E., Walega, J., Weibring, P., and Weinheimer, A. J.: Nitrogen dioxide and formaldehyde measurements from the GEOstationary Coastal and Air Pollution Events (GEO-CAPE) Airborne Simulator over Houston, Texas, Atmos. Meas. Tech., 11, 5941–5964, https://doi.org/10.5194/amt-11-5941-2018, 2018.

Pfister, G. G., Walters, S., Lamarque, J.-F., Fast, J., Barth, M. C., Wong, J., Done, J., Holland, G., and Bruyère, C. L.: Projections of future summertime ozone over the U.S., J. Geophys. Res.-Atmos., 119, 5559–5582, https://doi.org/10.1002/2013JD020932, 2014.

Pickering, K. E., Bucsela, E., Allen, D., Ring, A., Holzworth, R., and Krotkov, N.: Estimates of lightning NO_x production based on OMI NO_2 observations over the Gulf of Mexico, J. Geophys. Res.-Atmos., 121, 8668–8691, https://doi.org/10.1002/2015JD024179, 2016.

Platt, U.: Differential optical absorption spectroscopy (DOAS), in: Air Monitoring by Spectroscopic Techniques, edited by: Sigrist, M. W., Chemical Analysis Series, Vol. 127, John Wiley & Sons, Inc., 1994.

Pleim, J. E.: A Combined Local and Nonlocal Closure Model for the Atmospheric Boundary Layer. Part II: Application and Evaluation in a Mesoscale Meteorological Model, J. Appl. Meteorol. Clim., 46, 1396–1409, https://doi.org/10.1175/JAM2534.1, 2007.

Pleim, J. E. and Xiu, A.: Development of a Land Surface Model. Part II: Data Assimilation, J. Appl. Meteorol., 42, 1811–1822, https://doi.org/10.1175/1520-0450(2003)042<1811:DOALSM>2.0.CO;2, 2003.

Richter, A., Burrows, J. P., Nüß, H., Granier, C., and Niemeier, U.: Increase in tropospheric nitrogen dioxide over China observed from space, Nature, 437, 129–132, https://doi.org/10.1038/nature04092, 2005.

Ridley, B. A. and Grahek, F. E.: A small, low flow, high sensitivity reaction vessel for NO chemiluminescence detectors, J. Atmos. Ocean. Tech., 7, 307–311, https://doi.org/10.1175/1520-0426(1990)007<0307:ASLFHS>2.0.CO;2, 1990.

Russell, A. R., Valin, L. C., Bucsela, E. J., Wenig, M. O., and Cohen, R. C.: Space-based constraints on spatial and temporal patterns of NO_x emissions in California, 2005–2008, Environ. Sci. Technol., 44, 3608–3615, https://doi.org/10.1021/es903451j, 2010.

Russell, A. R., Valin, L. C., and Cohen, R. C.: Trends in OMI NO_2 observations over the United States: effects of emission control technology and the economic recession, Atmos. Chem. Phys., 12, 12197–12209, https://doi.org/10.5194/acp-12-12197-2012, 2012.

Ryerson, T. B., Williams, E. J., and Fehsenfeld, F. C.: An efficient photolysis system for fast-response NO_2 measurements, J. Geophys. Res., 105, 26447–26461, https://doi.org/10.1029/2000JD900389, 2000.

Saide, P. E., Kim, J., Song, C. H., Choi, M., Cheng, Y., and Carmichael, G. R.: Assimilation of next generation geostationary aerosol optical depth retrievals to improve air quality simulations, Geophys. Res. Lett., 41, 9188–9196, https://doi.org/10.1002/2014GL062089, 2014.

Saide, P. E., Gao, M., Lu, Z., Goldberg, D., Streets, D. G., Woo, J.-H., Beyersdorf, A., Corr, C. A., Thornhill, K. L., Anderson, B., Hair, J. W., Nehrir, A. R., Diskin, G. S., Jimenez, J. L.,

Nault, B. A., Campuzano-Jost, P., Dibb, J., Heim, E., Lamb, K. D., Schwarz, J. P., Perring, A. E., Kim, J., Choi, M., Holben, B., Pfister, G., Hodzic, A., Carmichael, G. R., Emmons, L., and Crawford, J. H.: Understanding and improving model representation of aerosol optical properties for a Chinese haze event measured during KORUS-AQ, Atmos. Chem. Phys. Discuss., https://doi.org/10.5194/acp-2019-1022, in review, 2019.

Schaub, D., Brunner, D., Boersma, K. F., Keller, J., Folini, D., Buchmann, B., Berresheim, H., and Staehelin, J.: SCIAMACHY tropospheric NO_2 over Switzerland: estimates of NO_x lifetimes and impact of the complex Alpine topography on the retrieval, Atmos. Chem. Phys., 7, 5971–5987, https://doi.org/10.5194/acp-7-5971-2007, 2007.

Schenkeveld, V. M. E., Jaross, G., Marchenko, S., Haffner, D., Kleipool, Q. L., Rozemeijer, N. C., Veefkind, J. P., and Levelt, P. F.: In-flight performance of the Ozone Monitoring Instrument, Atmos. Meas. Tech., 10, 1957–1986, https://doi.org/10.5194/amt-10-1957-2017, 2017.

Schreier, S. F., Richter, A., Schepaschenko, D., Shvidenko, A., Hilboll, A., and Burrows, J. P.: Differences in satellite-derived NO_x emission factors between Eurasian and North American boreal forest fires, Atmos. Environ., 121, 55–65, https://doi.org/10.1016/j.atmosenv.2014.08.071, 2015.

Skamarock, W. C., Klemp, J. B., Dudhia, J., Gill, D. O., Barker, D. M., Wang, W., and Powers, J. G.: A description of the Advanced Research WRF version 3. NCAR Technical note -475+STR, NCAR, Boulder, Colorado, USA, 2008.

Sluis, W. W., Allaart, M. A. F., Piters, A. J. M., and Gast, L. F. L.: The development of a nitrogen dioxide sonde, Atmos. Meas. Tech., 3, 1753–1762, https://doi.org/10.5194/amt-3-1753-2010, 2010.

Spinei, E., Cede, A., Swartz, W. H., Herman, J., and Mount, G. H.: The use of NO_2 absorption cross section temperature sensitivity to derive NO_2 profile temperature and stratospheric–tropospheric column partitioning from visible direct-sun DOAS measurements, Atmos. Meas. Tech., 7, 4299–4316, https://doi.org/10.5194/amt-7-4299-2014, 2014.

Steinbacher, M., Zellweger, C., Schwarzenbach, B., Bugmann, S., Buchmann, B., Ordóñez, C., Prevot, A. S. H., and Hueglin, C.: Nitrogen oxide measurements at rural sites in Switzerland: Bias of conventional measurement techniques, J. Geophys. Res.-Atmos., 112, D11307, https://doi.org/10.1029/2006JD007971, 2007.

Strahan, S. E., Douglass, A. R., and Newman, P. A.: The contributions of chemistry and transport to low arctic ozone in March 2011 derived from Aura MLS observations, J. Geophys. Res.-Atmos., 118, 1563–1576, https://doi.org/10.1002/jgrd.50181, 2013.

Strahan, S. E., Douglass, A. R., and Steenrod, S. D.: Chemical and dynamical impacts of stratospheric sudden warmings on Arctic ozone variability, J. Geophys. Res.-Atmos., 121, 11836–11851, https://doi.org/10.1002/2016JD025128, 2016.

Strode, S. A., Rodriguez, J. M., Logan, J. A., Cooper, O. R., Witte, J. C., Lamsal, L. N., Damon, M., Aartsen, B. V., Steenrod, S. D., and Strahan, S. E.: Trends and variability in surface ozone over the United States, J. Geophys. Res.-Atmos., 120, 9020–9042, https://doi.org/10.1002/2014JD022784, 2015.

Tewari, M., Chen, F., Wang, W., Dudhia, J., LeMone, M., Mitchell, K., Ek, M., Gayno, G., Wegiel, J., and Cuenca, R.: Implementation and verification of the unified NOAH land surface model in the WRF model, vol. 1115, American Meteorological Society, Seattle, Washington, USA, 2004.

Thornton, J. A., Wooldridge, P. J., and Cohen, R. C.: Atmospheric NO_2: in situ laser-induced fluorescence detection at parts per trillion mixing ratios, Anal. Chem., 72, 528–539, https://doi.org/10.1021/ac9908905, 2000.

Tzortziou, M., Herman, J. R., Cede, A., Loughner, C. P., Abuhassan, N., and Naik, S.: Spatial and temporal variability of ozone and nitrogen dioxide over a major urban estuarine ecosystem, J. Atmos. Chem., 72, 287–309, https://doi.org/10.1007/s10874-013-9255-8, 2015.

Tzortziou, M., Parker, O., Lamb, B., Herman, J. R., Lamsal, L., Stauffer, R., and Abuhassan, N.: Atmospheric trace has (NO_2 and O_3) variability in South Korean coastal waters, and implications for remote sensing of coastal ocean color dynamics, Remote Sensing, 10, 1587, https://doi.org/10.3390/rs10101587, 2018.

Valin, L. C., Russell, A. R., and Cohen, R. C.: Variations of OH radical in an urban plume inferred from NO_2 column measurements, Geophys. Res. Lett., 40, 1856–1860, https://doi.org/10.1002/grl.50267, 2013.

van der A, R. J., Eskes, H. J., Boersma, K. F., Noije, T. P. C. v., Roozendael, M. V., Smedt, I. D., Peters, D. H. M. U., and Meijer, E. W.: Trends, seasonal variability and dominant NO_x source derived from a ten year record of NO_2 measured from space, J. Geophys. Res.-Atmos., 113, D04302, https://doi.org/10.1029/2007JD009021, 2008.

van Noije, T. P. C., Eskes, H. J., Dentener, F. J., Stevenson, D. S., Ellingsen, K., Schultz, M. G., Wild, O., Amann, M., Atherton, C. S., Bergmann, D. J., Bey, I., Boersma, K. F., Butler, T., Cofala, J., Drevet, J., Fiore, A. M., Gauss, M., Hauglustaine, D. A., Horowitz, L. W., Isaksen, I. S. A., Krol, M. C., Lamarque, J.-F., Lawrence, M. G., Martin, R. V., Montanaro, V., Müller, J.-F., Pitari, G., Prather, M. J., Pyle, J. A., Richter, A., Rodriguez, J. M., Savage, N. H., Strahan, S. E., Sudo, K., Szopa, S., and van Roozendael, M.: Multi-model ensemble simulations of tropospheric NO_2 compared with GOME retrievals for the year 2000, Atmos. Chem. Phys., 6, 2943–2979, https://doi.org/10.5194/acp-6-2943-2006, 2006.

Vandaele, A. C., Hermans, C., Simon, P. C., Carleer, M., Colin, R., Fally, S., Mérienne, M. F., Jenouvrier, A., and Coquart, B.: Measurements of the NO_2 absorption cross-section from 42 000 cm^{-1} to 10 000 cm^{-1} (238–1000 nm) at 220 K and 294 K, J. Quant. Spectrosc. Ra., 59, 171–184, https://doi.org/10.1016/S0022-4073(97)00168-4, 1998.

Vasilkov, A., Qin, W., Krotkov, N., Lamsal, L., Spurr, R., Haffner, D., Joiner, J., Yang, E.-S., and Marchenko, S.: Accounting for the effects of surface BRDF on satellite cloud and trace-gas retrievals: a new approach based on geometry-dependent Lambertian equivalent reflectivity applied to OMI algorithms, Atmos. Meas. Tech., 10, 333–349, https://doi.org/10.5194/amt-10-333-2017, 2017.

Vasilkov, A., Yang, E.-S., Marchenko, S., Qin, W., Lamsal, L., Joiner, J., Krotkov, N., Haffner, D., Bhartia, P. K., and Spurr, R.: A cloud algorithm based on the O2-O2 477 nm absorption band featuring an advanced spectral fitting method and the use of surface geometry-dependent Lambertian-equivalent reflectivity, Atmos. Meas. Tech., 11, 4093–4107, https://doi.org/10.5194/amt-11-4093-2018, 2018.

Veefkind, J. P., de Haan, J. F., Sneep, M., and Levelt, P. F.: Improvements to the OMI O_2–O_2 operational cloud algorithm and comparisons with ground-based radar–lidar observations, Atmos. Meas. Tech., 9, 6035–6049, https://doi.org/10.5194/amt-9-6035-2016, 2016.

Vinken, G. C. M., Boersma, K. F., van Donkelaar, A., and Zhang, L.: Constraints on ship NO_x emissions in Europe using GEOS-Chem and OMI satellite NO_2 observations, Atmos. Chem. Phys., 14, 1353–1369, https://doi.org/10.5194/acp-14-1353-2014, 2014.

Vlemmix, T., Piters, A. J. M., Stammes, P., Wang, P., and Levelt, P. F.: Retrieval of tropospheric NO_2 using the MAX-DOAS method combined with relative intensity measurements for aerosol correction, Atmos. Meas. Tech., 3, 1287–1305, https://doi.org/10.5194/amt-3-1287-2010, 2010.

Wang, S. W., Zhang, Q., Streets, D. G., He, K. B., Martin, R. V., Lamsal, L. N., Chen, D., Lei, Y., and Lu, Z.: Growth in NO_x emissions from power plants in China: bottom-up estimates and satellite observations, Atmos. Chem. Phys., 12, 4429–4447, https://doi.org/10.5194/acp-12-4429-2012, 2012.

WHO: Review of evidence on health aspects of air pollution REVIHAAP Project, Tech. rep., 302 pp., World Health Organization, Copenhagen, Denmark, available at: http://www.euro.who.int/__data/assets/pdf_file/0004/193108/REVIHAAP-Final-technical-report-final-version.pdf?ua=1 (last access: 5 September 2019), 2013.

Wild, R. J., Edwards, P. M., Dubé, W. P., Baumann, K., Edgerton, E. S., Quinn, P. K., Roberts, J. M., Rollins, A. W., Veres, P. R., Warneke, C., Williams, E. J., Yuan, B., and Brown, S. S.: A measurement of total reactive nitrogen, NOy, together with NO_2, NO, and O_3 via cavity ring-down spectroscopy, Environ. Sci. Technol., 48, 9609–9615, https://doi.org/10.1021/es501896w, 2014.

Wong, D. C., Pleim, J., Mathur, R., Binkowski, F., Otte, T., Gilliam, R., Pouliot, G., Xiu, A., Young, J. O., and Kang, D.: WRF-CMAQ two-way coupled system with aerosol feedback: software development and preliminary results, Geosci. Model Dev., 5, 299–312, https://doi.org/10.5194/gmd-5-299-2012, 2012.

Yarwood, G., Rao, S., Yocke, M., and Whitten, G.: Updates to the Carbon Bond Chemical Mechanism: CB05. RT-0400675, vol. 8, U.S. Environmental Protection Agency, Washington, District of Columbia, USA, 2005.

Zhao, C. and Wang, Y.: Assimilated inversion of NO_x emissions over east Asia using OMI NO_2 column measurements, Geophys. Res. Lett., 36, L06805, https://doi.org/10.1029/2008GL037123, 2009.

Zhou, D. K., Larar, A. M., Liu, X., Smith, W. L., Strow, L. L., Yang, P., Schlussel, P., and Calbet, X.: Global Land Surface Emissivity Retrieved From Satellite Ultraspectral IR Measurements, IEEE T. Geosci. Remote, 49, 1277–1290, https://doi.org/10.1109/TGRS.2010.2051036, 2011.